A STUDY OF FRACTURE MECHANISMS IN ATD ROLLER BEARING

Ralph Zee, Principal Investigator

Abstract

A research project was conducted to study the relationships between microstructure, residual stress and mechanical behavior in 440C bearing materials. The purpose of this study is to investigate how microstructures, especially anisotropy, affects internal stresses and the overall mechanical response of the bearing. Anisotropy includes both the aligned carbide distribution and the grain orientation. Mechanical properties as a function of orientation of the sample were measured using small tensile samples heat treated accordingly. Samples with the stress axis along the aligned carbide direction possessed high modulus values compared to those with their axis perpendicular to the carbide stringers. The difference in the modulus was found to be more than a factor of 2. A series of experiments was conducted on rolled samples to further investigate this effect and the two sets of results were consistent with each other. The degree of anisotropy of the microstructure in terms of the carbide and matrix orientations was determined using x-ray diffraction. The stress state determination was conducted using neutron diffraction. It was found that there was little variation in the distribution of the internal stresses amongst different samples indicating that small changes in the processing and geometrical conditions did not result in significant variations in the internal stress. A nominal tensile hoop stress of 30 ksi was obtained for the inner raceway. Furthermore, during the course of the investigation, it was apparent that there was a need to determine the stress state induced by the shrink fitting process. Therefore, a series of experiments was conducted using strain gages to identify the

(NASA-CR-184200) A STUDY OF FRACTURE MECHANISMS IN ATD ROLLER BEARING Final Report, 6 Jun. 1989 - 5 Sep. 1990 (Auburn Univ.) 58 p

N91-32497

CSCL 13I

Unclas

G3/37 0040118

stress distribution in a shrink fitting process in three different types of geometries and correlation were obtained to estimate the highest stress values in an outer and an inner groove geometry. A finite element program based on the ANSYS system was developed to compute the stress distribution in the inner raceway geometry. This analysis indicates that the highest tensile stress in the system occurs at the ID of the ring with a stress value of over 5 times that of the applied radial stress. Results from all these facets were correlated with one another. It appears that the material does not fail as a result of any one single factor but a combination of the various effects investigated.

I. Introduction

The ATD bearings are designed for use in the turbo pumps in cryogenic engines and must be able to endure high revolution rates, high stress and moderate temperature cycling (from cryogenics to ambient). These bearings must be made of steels which possess high strength and high wear resistance. Martensitic steels have these attributes. However, they are also very brittle and have little impact resistance. Pratt Whitney is the main contractor of NASA for this component. Some rings were found to crack prematurely below the expected tensile stress of the materials and some rings showed surface microcracks as reviewed by die penetrant examination. For this component to function properly in the turbo pumps, it is imperative that solution be found to eliminate this cracking problem.

There are presently two ideas as to the origin of the crack generation. One is the residual stress in the component which is produced during the complex fabrication stages. This residual stress could be tensile in nature

which could lead to the catastrophic cracking. This residual stress can be a combination bulk and surface states. The second possible cause is due to the presence of aligned carbides. In detailed metallographic examinations, it was found that the carbides appeared in a non-random manner. Their presence in such a morphology may have severely reduced the tensile property of the materials in certain direction. This weakness combined with internal stresses most likely have caused the ring to fail after fabrication even without any externally applied stresses.

II. Objectives and Limitations of Present Understanding

It is the purpose of this twelve-month research to investigate the contributing factors to the failure of bearing materials. This project was extended by three months via a no-cost extension. Emphases of the project were placed on:

a. The effects of orientation on tensile mechanical properties. This was investigated by cutting tensile specimens of different orientations from the bar stock and testing these specimens to determine their respective mechanical properties.

b. The anisotropy of the carbides and the matrix. X-ray diffraction patterns were determined for the specimens cut from different orientation of the bar stock. The relative intensity of the peaks is related to probability of the orientation and therefore an indication of the texture of the material. The role of the aligned carbides (also called stringers) were investigated. The objective here is to examine the anisotropic response in the mechanical properties (or lack of it) due to the presence of these anisotropically distributed carbides.

c. The role of bulk residual stress. The level and state of the residual stress generated by the fabrication process of the bearings were investigated. The role of residual stress was addressed using neutron diffraction. Results from earlier x-ray diffraction analysis show that tensile stresses exist just beneath the outer surface of the ring. However, the stress state measured using x-ray is limited to the surface region which is not representative of the bulk state. Furthermore, x-ray also produces tremendous amount of florescence in steels and this leads to excessive background in the detector. In this study, neutron was used to measure the true bulk residual stress in bearing components. The IPNS (Intensed Pulsed Neutron Source) neutron diffractometer at Argonne National Laboratory was used for this purpose. This national facility is open to public user based on scientific merit of the experiment. Results from this neutron diffraction study provide information on the bulk residual stress as a function of position inside the ring.

d. The stress generated in a shrink fitting process. A method based on strategic location of strain gages was developed and the surface stress (tensile in the hoop direction) was determined experimentally during the fitting and the stress relaxation processes. Three geometries were conducted to test this method and results were very encouraging.

e. The analysis of shrink fitting stress using finite element. A finite element analysis program based on ANSYS was developed to calculate the stress distribution generated by shrink fitting.

It is probable that it is the combination of the residual stresses and the aligned carbide that leads to the catastrophic cracking. For example, one

possibility is that the magnitude of the bulk residual stress is not high enough to produce the failure but the presence of the aligned carbides severely degrade the properties in the direction of the tensile stress and lead to premature cracking. In this study, all the information (including available from other sources) was reviewed to elucidate the cause of the failure.

III. Results of the Project

This is a one-year project to investigate in a preliminary manner all the contributing factors affecting premature cracking in bearing materials. Results from this one year study will be presented in the five categories as illustrated in the above section.

a. The effects of orientation on tensile mechanical properties. This was investigated by cutting tensile specimens of different orientation from the bar stock and testing these specimens to determine their respective mechanical properties. Tensile specimens were fabricated from bar stock in different directions to study the effects of anisotropy on tensile properties and structure. Two quarters of a 440C bar stock were obtained from NASA. These two pieces were in the as-extruded condition. A total of 24 tensile specimens were fabricated and tested at room temperature. Each tensile specimens possessed a gage length of 1", a thickness of 1/8" and a gage width of 3/16". The grip area measured 5/16"x5/16". This miniature configuration was chosen due to the limitation of the size and the shape of the bar stock. All the specimens tested were first machined in the as-received condition and then underwent the heat treatment to attain the hardness required. A Centorr vacuum furnace was modified to perform insitu quenching directly from high

temperature into oil to generate the necessary martensitic transformation. A vacuum better than 10^{-6} torr was maintained at all times. The specimens were first preheated inside the vacuum furnace to 1500°F for 30 minutes and then austenitized at 1965°F for 1 hour. They were then oil quenched and then subzero treated at -100°F (in freezer) for 2 hours, warmed to room temperature and tempered at 335°F for 2 hours. This was followed by a second subzero treatment at -100°F and cooled in liquid nitrogen for 2 hours. The specimens were cooled in dry nitrogen to ambient and then received a final temper at 335°F for 2 hours and then air cooled. Microhardness measurements were made at various locations of each of the 24 tensile specimens during all stages of the heat treatment process. The inter-specimens values at each stage were very consistent indicating the reproducibility of the process. In this report, only the final hardness values will be given. All other values can be supplied upon request.

Two groups of specimens were tested. Specimens from Group A were cut directly from the bar stock from positions and orientation as illustrated in figure 1. This group is composed of specimens A, B, C, D, E, F and 9 through 18. All these 16 specimens, with the exception of specimen A, were cut and tested with the gage length along the axial direction of the bar. Three plates were cut in this group (Plates 1, 2 and 3). Results from these tests indicate a tremendous weakening of the tensile property in specimen A due to its orientation. Group B consists of specimens 1 through 8. In this group, a sheet was first cut from one of the two flat faces of the bar and then cold rolled 30% in the directly shown in figure 2. This rolling direction was parallel to specimens 1 through 5 and perpendicular to specimens 6, 7 and 8. As shown in the results that follow, this led to a variation in the tensile

property.

Table 1 summarizes the results from this mechanical testings. Unfortunately specimens D, 2, 3 and 7 failed prematurally during test due to slippage of the grip and no useful data were obtained. The Rockwell hardness measurements revealed that the hardness values ranged consistently from R_C of 55.5 to 57.9. These are slightly below the desired values of 58. This discrepancy is most likely a result of calibration more than real difference.

In Group A Plate 1, specimen A possessed the weakest modulus among all specimens tested (only 13.2 Msi which was less than 50% of the average). This strongly indicates the dependence of the tensile property with orientation. The carbide stringers were found to be arranged in a circumferential manner which suggested that the weakest direction should be in the radial direction in accord with our present finding. Furthermore, the anisotropy of the stringers was determined to be strongest near the circumference. In Group A, specimens B through F, 9 through 13 and 14 through 18 were respectively cut from the circumferential position inward. As illustrated in Table 1, specimens B through F possessed progressive lower modulus from 33.4 to 27.5 Msi. Similarly, specimens 9 through 13 had decreasing moduli from 30 to 27.5 Msi. However, specimens 14 through 18 exhibited less of a clear trend. This is due to the fact that these specimens were cut from a less symmetrical block as illustrated in figure 1.

Specimens in Group B were made from a plate which had been cold rolled 50% as shown in figure 2. This cold work was performed prior to the heat treatment process. Tensile results, given in Table 1 again illustrate the dependence of tensile modulus on cold work direction. Working is expected to produce aligned carbides along the direction of the deformation, which in this

case along the gage length of specimens 1 through 5, but perpendicular to specimens 6, 7 and 8. Unfortunately, specimens 2, 3 and 7 failed prematurally. Nevertheless, it is evident from the results given in Table 1 that the specimens with the aligned carbides (specimens 1, 4 and 5) possessed higher moduli than those with the carbides lying perpendicularly to the test direction (specimens 6 and 8). The average modulus for specimens 1, 4 and 5 was 43 Msi as opposed to a value of 30.4 Msi for specimens 6 and 8. This difference in the modulus is due to the alignment of the carbides relative to the applied stress direction.

Table 1: Tensile Tests Results

	Specimen No.	Rockwell Hardness	Tensile Modulus (Msi)
	A	56.2	13.2
	B	57.9	33.4
Group A	C	57.1	32.0
Plate 1	D	(Failed prematurally)	----------
	E	57.9	28.7
	F	57.6	27.5
	9	57.5	30.0
	10	56.3	29.1
Group A	11	56.7	28.9
Plate 2	12	57.1	28.1
	13	57.0	27.5
	14	56.2	28.3
Group A	15	56.3	27.1
Plate 3	16	56.2	26.6
	17	57.2	26.6
	18	57.0	27.0
	1	56.6	42.6
	2	(Failed prematurally)	----------
	3	(Failed prematurally)	----------
Group B	4	56.2	46.2
	5	56.7	41.9
	6	55.5	30.4
	7	(Failed prematurally)	----------
	8	56.2	30.4

b. The anisotropy of the carbides and the matrix. X-ray diffraction patterns were determined for all the specimens cut from different orientation of the bar stock that were used in the mechanical testing described above. A Rigaku DMAX-B theta theta vertical diffractometer was used for this study. The two-theta angles used were from 30° to 90° with a scan rate of 5°/min which was found to be adequate for most applications. The divergent and scattering slits were both 1° and the receiving slit was 0.15 mm. Three patterns were taken from each specimen. The first, denoted as longitudinal, was taken from the flat surface of the gage section. The second, denoted as long transverse, was taken from the size surface of the gage section. The third, denoted as short transverse, was taken from the cross sectional area of the gage section. The relative intensity of the peaks is related to probability of the orientation and therefore an indication of the texture of the material. Figures 3 through 25 give the diffraction patterns taken.

This preliminary study do not permit any detailed investigation of the pattern obtained. However, a scan of the result indicates that there exists a direct correlation between the orientation of the specimens with their diffraction patterns. A comparison of the three patterns (in the longitudinal, long transverse and short transverse directions) from any one of the 24 samples clearly reveals signification variations of the peak intensities indicating differences in the carbide concentration and texture. In addition, there also exists variations in the patterns obtained from samples cut from different positions of the bar stock as well as the samples undergone cold rolling. A more detailed and systematic study is required to determine a definitive correlation between texture, morphology and properties.

c. The role of bulk residual stress. Two sets of neutron diffraction experiments were conducted at the IPNS system operated by the Argonne National Laboratory. These IPNS experiments are part of a multifacet program which is aimed at understanding the fracture and stress behavior in 440C steels. The goal is to identify the bulk residual stress state as a function of position.

In the first set of experiments, eleven runs were conducted on 10 specimens (the standard was run twice to ensure reproducibility) using a position resolving geometry. The detector banks at +148°, +60° and +90° were activated and time focussed. A 1.5mm entrance slit was placed 4.6cm in front of the sample and a 1mm exit slit was placed at 8cm away in the -90° arm. The geometry established by the two slits and the positioning of the sample ring provide position sensitivity using the 20 detectors at -90°. These 20 detectors were tied in sets of 4 each (5 sets for 5 positions) and 2 each (10 sets for 10 positions). The former was found to be more acceptable due to higher count rates. Using the geometry of this experiment, stress in volume spaced as close as 1.5mm can be resolved. Position 1 at -90° represents the analysis volume near the outer surface of the ring whereas position 5 represents the volume near the inner surface. It is important to point out that the neutrons diffracted into the detectors with negative angles are biased towards the Bragg planes with their normals near the circumferential direction whereas the detectors with positive angles examine the planes with their normals near the radial direction. Due to the ring geometry of these samples, it is logical to assume to that the main principal stress is the circumferential hoop stress.

Table 2 summarizes the results whereas Table 3 shows the strain values in

percent converted from the d-spacing measurements from the -90° detectors. The numbers represent the tempering temperatures in degrees Fahrenheit. BB represents ball bearing configuration which is slightly different than the rest of the sample and PF represents the pancake forged condition, which gives a different carbide distribution. A thin sheet (1.3 mm thick) was used as standard. This was used instead of powder or small cube cut from the ring specimen due to the difficulty involved in preparation as a result of the hardness of this material. All the values given are in angstrom. Using the -90° detectors and the configuration of the defining slits, strain measurements through the radial direction were obtained. Position 1 at -90° represents the analysis volume near the outer surface of the ring whereas position 5 represents the volume near the inner surface. The planes analyzed in the -90° detectors are those with their normals in the radial direction.

The last two entries in Table 2 (Clamped and Clamp-AL) were two samples that were clamped to introduce known stress state in the ring. Unfortunately it was later found that the clamp condition was inappropriate for this purpose and the results were not analyzed.

Table 2. Summary of d-spacing results from the first set of experiments.

Specimen	+148°	-148°	+60°	-60°	+90°	Position Resolving at -90°				
						Outside		Middle		Inside
						1	2	3	4	5
Standard	2.0392	2.0389	2.0399	2.0409	2.0383	thin sheet not position resolved				
325°F	2.0375	2.0371	2.0383	2.0371	2.0381	2.0370	2.0368	2.0369	2.0366	2.0360
900°F	2.0360	2.0358	2.0372	2.0372	2.0372	2.0367	2.0355	2.0354	2.0357	2.0340
600°F	2.0366	2.0364	2.0373	2.0360	2.0377	2.0374	2.0357	2.0359	2.0353	2.0345
450°F	2.0376	2.0373	2.0391	2.0378	2.0391	2.0401	2.0373	2.0367	2.0366	2.0360
350°F	2.0382	2.0382	2.0402	2.0387	2.0401	2.0410	2.0375	2.0385	2.0376	2.0370
350°F-BB	2.0375	2.0371	2.0379	2.0371	2.0379	2.0377	2.0361	2.0367	2.0354	2.0345
350°F-PF	2.0370	2.0372	2.0367	2.0368	2.0370	2.0342	2.0372	2.0357	2.0358	2.0350
Clamped	2.0372	2.0365	2.0367	2.0354	2.0369	2.0354	2.0358	2.0365	2.0356	2.0350
Clamp-AL	2.0246	2.0235	2.0228	2.0224	2.0251	2.0252	2.0274	2.0258	2.0274	2.0250

Table 3. Summary of strain calculated from the position resolving detectors at -90°

Specimen	Position Resolving at -90° (%strain)				
	Outside		Middle		Inside
	1	2	3	4	5
325°F	0.017	0.007	0.012	-0.003	-0.032
900°F	0.061	0.002	-0.003	0.012	-0.072
600°F	0.081	-0.003	0.007	-0.023	-0.060
450°F	0.135	-0.002	-0.031	-0.036	-0.060
350°F	0.111	-0.040	0.009	-0.035	-0.046
350°F-BB	0.080	0.001	0.030	-0.033	-0.077
350°F-PF	-0.092	0.055	-0.018	-0.013	-0.053

Due to the geometry of the first experiment, it is only possible to obtain the strain in the planes with their normals parallel to the radial direction of the ring. This limits the completeness of the interpretation of the stress state. A meeting with the NASA and the Pratt and Whitney scientists was held at MSFC to discuss future experiments. As a result of this meeting, a new proposal to the Argonne National Laboratory was submitted to request free beam time on the IPNS for a second round of experiment. This set of experiments will investigate other Bragg planes to elucidate the triaxial stress state in

the ring. This proposal to the IPNS was accepted and four days of beam time on the instrument was allocated to us.

In addition a new specimen holder was designed at Auburn which facilitated simultaneous determination of six sets of Bragg planes. This holder was expected to enhance the statistics dramatically in the second IPNS experiment. A second set of experiments was conducted at the Intensed Pulsed Neutron Source at Argonne National Laboratory to further analyze the bulk stresses in 440C materials. A total of 21 runs were performed on six specimens (including references and standards). The experimental arrangement for these experiments was different than that in the first set. In the first set of experiments, the strain in the planes with their normals in the radial direction was examined. However, in the case of hoop stress, it is necessary to examine also the circumferential strain so that more precise stress analysis can be performed. To accomplish this, it is best to place the exit slit in the 90° arm. Unfortunately, this means that significant absorption would have taken place resulting in unacceptable counting rates. After discussing the problems with ANL, NASA and Pratt-Whitney scientists, it was decided that a new geometry will be used. Present configuration of the setup at ANL only permits one bank of detectors to be used in the position sensitive mode. A sample holder plate with manual slits for all banks detectors (±90, ±60 and ±148) was designed and fabricated. The locations for the six slits were chosen so that the detectors at each bank see the entire length of the sample. This new geometry essentially collects six sets of usable data instead of one during each experiment.

In this second run at IPNS, specimens were supplied by Dr. Chin and Mr. Samuelson of Pratt-Whitney. To examine the size effects in the second set of

experiments, two ring thicknesses, 6 mm and 9 mm, were used. A number of runs were conducted using an upright geometry of the specimen rings. In this configuration, the position defining slits were all removed. All the detectors at the six angles were activated. This allows the analysis of the Bragg planes which are normal to the tradition sets. These experiments were successful with little beam interruptions. The more sophisticated arrangement in this second set of experiments permits a more detailed analysis of the stress state. As a result of this second set of experiments, an extensive amount of data was generated. At the conclusion of this project, there still remains a fraction of these data to be analyzed. Table 4 summaries the results from two sample rings analyzed using the position resolving method. The ring denoted as 3-7 was a roller bearing inner race whereas the 6MM sample was a 6mm thick ring without the raceway. Both rings were processed using the traditional routine. In this table, only the detectors at +90° and -90° were given. Results from the other four banks (+148°, -148°, +60° and -60°) were also analyzed but will not be included for the sake of simplicity. Table 5 provides the conversion of the d-spacings to lattice strains which are related to the stress via the Possion ratio and the Young's modulus. Table 6 gives the strain values determined from the experiments using the upright position without the position defining slits.

Table 4. Summary of d-spacing results from the second set of experiments.

	Position Resolving at +90°					Position Resolving at -90°				
Spec	Outside		Middle		Inside	Outside		Middle		Inside
	1	2	3	4	5	1	2	3	4	5
3-7	*	*	2.0406	2.0380	2.0382	2.0383	2.0381	2.0389	2.0379	2.0380
6MM	2.0395	2.0394	2.0394	2.0393	2.0384	2.0397	2.0390	2.0394	2.0384	2.0385

Table 5. Summary of strain calculated from the position resolving detectors at +90° and -90° (Values in the table are in % strain)

Spec	Position Resolving at +90°					Position Resolving at -90°				
	Outside		Middle		Inside	Outside		Middle		Inside
	1	2	3	4	5	1	2	3	4	5
3-7	*	*	0.116	-0.012	-0.002	0.003	-0.007	0.032	-0.017	-0.012
6MM	0.015	0.010	0.010	0.005	-0.039	0.034	0.000	0.020	-0.029	-0.025

Table 6. Summary of strain calculated from the experiment using an upright geometry

Specimen	Detector Set		
	148 (%)	90 (%)	60 (%)
3-7 (Outside)	-0.050	0.001	0.048
(Middle)	-0.035	-0.002	0.038
(Inside)	-0.047	-0.015	0.076
6MM (Outside)	-0.010	0.002	0.002
(Middle)	-0.030	-0.013	0.040
(Inside)	-0.050	-0.025	0.102

Results from the position resolving detectors at -90° from both sets of experiments clearly show that there exists a gradient in the hoop stress as a function of radial position. The inner surface (detector 5) in all the rings possessed the strongest negative strain values. Assuming that the dominant stress is hoop in nature, this result indicates that the inside surface has the highest hoop tensile stress. This phenomenon is in accord with the stress expected from the volume change due to martensitic transformation. Other results from these two sets of experiments are in qualitative agreeement with stress generation due to martensitic transformation. However, as evident from the scatter of the data, a more quantitative analysis at this time is

unwarranted. The scatters in the data are partly due to the low counting statistics and in part due to the lack of the baseline value for the stress-free 440C lattice parameter. This reference value is usually obtained experimentally using powder made from the bulk. Unfortunately, in our case, the making of the powder is impossible due to the high hardness of the material. The conversion of d-spacings to strain was obtained using an estimated equilibrium lattice parameter based on the average of all the values obtained. It was also found that higher tempering temperatures did not reduce the amount of residual stress (or stress gradient). The 440C steel is a multiphase alloy. The higher tempering temperature may relieve some residual stress induced by quenching, but it also inevitably lead to larger internal stresses by differential thermal contraction of the various phases.

Albeit a full quantitative analysis was not possible at this time, it is pausible to estimate the stress level in the ring. In all the configurations used in both the first and the second sets of the experiments, the hoop strain was never measured directly due to the unfortunately inherent geometrical limitation. It is reasonable to expect that the dominant stress will be hoop in nature. With this assumption, the strain values measured in all the experiments are related to the hoop stress via the Possion ratio. A scan through the data indicate that the highest strain values were observed in the inside of the ring. Using a measured value of -0.03% strain in the inside surface for the Bragg plane with its normal in the radial direction, a hoop stress of approximately 30 ksi was calculated.

d. The stress generated in a shrink fitting process. In most of the shrink fitting process, the stress distribution in the inner raceway of the bearing

was calculated using the simple stress determination based on a uniform cross sectional area. However in the real situation, the cross sectional area is not simple rectangular in shape but rather of some complex geometries. In this section of the study, an experimental determination of the surface stress (or strain) was developed based on the strategic location of strain gages during the fitting and the stress relaxation processes. Three geometries were conducted to test this method and results were very encouraging. Figures 26a, b and c provide the three types of geometry used. The main variables examined include material (aluminum and stainless steel), configuration (plain rectangular cross section, inner groove and outer groove), and tolerance. These combinations provided parameter control to determine the dominant factor in fit-induced stress.

There were a total of 17 test runs performed. In each experiment, three strain gages were strategically placed at different locations and in different orientations on the outer ring. The strains induced in these gages were continuously monitored during the heating, fitting, and shrinking processes. These measurements provided a direct determination of the stress induced by shrink fitting. Relaxation of this strain due to crack formation was investigated by slitting the ring using a diamond saw and monitoring the recovery of the strain gages.

In these experiments stresses induced by the shrink fitting process were measured by three strain gages located at strategic positions. The principle testing equipment consist of three battery powered strain indicators, one strip chart recorder, three 350 ohm resistance strain gages per sample ring, two thermocouples, one diamond saw, one sample test fixture, and one furnace. The two channel strip chart recorder was used to continuously monitor two of

the three strain gages. The strain gages were of the type that could tolerate a temperature of 200°C. The diamond saw was used for slitting the ring after fitting to examine stress relaxation. It was found upon execution that the crucial factor for success was timing. This being the time elapsed between the sample ring leaving the furnace, until the liquid nitrogen chilled shaft was inserted into the ring. To complete one successful test run took approximately two hours. The sample rings spent 30 minutes warming up in the 200°C furnace (which heated the ring's surface to a temperature between 160°C and 187°C), 30 seconds for the fit, between 45 minutes to one hour equilibrating to room temperature, and then between 15 to 45 minutes to initiate and propagate a crack on the samples outer surface depending on the ring wall thickness.

Results from this portion of the research project can be divided into three main areas according to the geometry of the samples as follows: (1) rings with uniform cross section, (2) rings with outer groove, and (3) rings with inner groove. Results from this study and their implications in the stress distribution of shrink fits will be presented accordingly.

Rings with Uniform Cross Section: A total of nine assemblies were tested under this category. In these tests, three variables were explored: material combination, tolerance and ring thickness. All rings were made of annealed aluminum with the shaft being either aluminum (2219Al) or stainless steel (303SS). Two ring thicknesses of 1/4" and 3/8" and four tolerance values of 0.003", 0.005", 0.0055", and 0.0065" were used. The tolerance levels refer to the misfit between the radius of the shaft and the inside radius of the ring. The purpose of the investigation using a simple uniform geometry is two-fold: one is to determine the validity of the calculations based on stress

mechanics, and the second is to verify the experimental approach and the accuracy of the measurements. In each of the test runs, three strain gages were attached to the outer surface of the ring as shown in Figure 3a. The nominal inside diameter of the ring was 2.25". Gages labelled TAN1 and TAN2 were placed on opposite sides of the ring, both measuring the strains in the tangential direction whereas, the gage labelled AXIAL was placed adjacent to gage TAN1 but measuring the axial strain. All the strain values were continuously monitored during the experiments. TAN1 and TAN2 consistently yielded similar results as expected. Their strains will be presented here as single tangential values (TAN). Results from the AXIAL gage will be referred to as "AXI".

Table 7 summarizes the results from this series of experiments. The equilibrium strains at the surface of the ring, both tangential and axial are given. The positive strain in the tangential direction is a direct consequence of the tensile hoop stress produced by the fitting process. According to the axial geometry of the assembly, there should be no axial stress generated. The negative axial strain measured by AXI is therefore a result of the Poisson ratio effect. Table 7 also includes calculated values for the tangential strain expected at the surface.

The main factors in the calculation of the strain level at the surface are materials parameter modulus, geometrical parameters and also the fitting tolerance delta (δ, that is the deformation induced in the ring as a result of the shrink fitting. Two methods were used in determining the delta values from the tolerances. In method 1, it was assumed that since the inner shaft

Table 7. Results for Rings with Uniform Cross Section.

Ring-Shaft, Wall Tolerance		AL-AL,1/4" 0.0055"	AL-AL,3/8" 0.005"	AL-AL,3/8" 0.0065"	AL-SS,3/8" 0.003"
As-Fitted	CAL1:	5852	4776	6209	2866
	CAL2:	2926	2388	3105	2102
	TAN:	2851	2327	2562	1379
	AXI:	-1542	-926	-967	-775
Prior to Failure	TAN:	2000	-300	0	250
	AXI:	-2200	-250	-250	-609
After Ring Failure	TAN:	-450	-94	86	200
	AXI:	-475	226	201	-597

*All values in this table are in microstrains.

is under compression radially, its deformation was insignificant and therefore all the tolerance misfit was accommodated by the delta (radial train in the ring). Strain values calculated using this assumption are given in Table 7 under the description CAL1. These values represent the upper limit of the strains, although they do not account for relaxation. However, it is obvious that the inner shaft does deform. In method 2, the relative amount of deformation between the ring and the shaft (δ_1/δ_2) should be prorated according to the ratio of the modulus between the ring (E_1) and the shaft (E_2) as follows:

$$\delta_1/\delta_2 = E_2/E_1$$

Tangential strains calculated based on the above delta are given in Table 7 under the entry CAL2. A direct comparison between the calculated values and the experimentally determined tangential strains indicate that measured tangential strains are always lower than the calculated values (even for

method 2). It appears that the calculated value based on method 1 where the entire misfit is accommodated by the ring grossly overestimate the surface tangential stress. The method of misfit partitioning based on equation (4) seems to be more appropriate. The larger degree of inconsistency between the experimental and the calculated values occurs in the assembly with the smallest tolerance (0.003"). This is because with such a small tolerance level, small variations in the machining accuracy and fitting procedure are magnified.

The strain relaxation due to slitting of the ring is given in Table 7. The rings were cut using a diamond saw between the two neighboring gages in the tangential and axial directions. In all the relaxation experiments, the strain values decreased during the cutting process. At a certain critical point where the tensile strength of the materials was attained (a progressive increase in stress due to a decreasing cross sectional area), the ring failed by fracture. The strain values before and after such critical fracture are given in the table. It is evident that for the rings with the larger tolerances the strain values decreased as expected upon cutting. However, the changes registered in the rings with 0.003" misfit (smallest) were more scattered. This again is due to the small value which introduces positional dependence of relaxation.

Rings with Outer Grooves: A total of four samples were tested under this geometry. Two material combinations were used: Al ring on Al shaft (Al-Al) and Al ring on SS shaft (Al-SS). In these sample assemblies, the geometry was fixed with a groove depth of 1/8" and a width of 1/2" with the overall thickness of the ring being 3/8". The total tolerance was maintained at 0.005". Three strain gages were placed on each ring at strategic locations as

illustrated in Figure 26b. Table 8 gives the experimental results from these assemblies. In both cases (Al-Al and Al-SS), the hoop strains in TAN2 located on the groove surface registered the highest values of between 2600 and 4000 microstrain. On the contrary the deformation on the outer surface (TAN1) was much lower, about 10-15% of TAN2 values. These outer surface stresses are also lower than those recorded in the smooth ring geometry presented in part A. Evidently, the presence of the groove results in a condition where the stress (and therefore the strain) is dissipated at the outer surface. The exact analytical determination of this relaxation is not possible. A finite element analysis using ANSYS was performed to determine the stress distribution in this geometry. Preliminary results indicate that the stress gradient at the groove surface was large. At the center of the groove there exists a tangential stress of approximately 40 ksi, corresponding to a tangential strain of 4000 microstrain in quantitative agreement with the experimentally observed data. Table 8 also includes calculated strain values using a simple uniform geometry with a ring thickness of 1/4". This value corresponds to the position of TAN2 located at the bottom of the groove. For Al on SS, the calculated the experimental values agree very well whereas the calculated value underestimated the data in the Al on Al geometry. This discrepancy is most likely due to the uncertainty involved in the strain measurement. The negative values for the axial strain are not due to an axial stress (since this does not exist in this experiment), but rather to the poisson ratio effect from the hoop strain. It is important to note that in this more complex geometry, the axial contraction does not scale exactly with the Poisson ratio. This contraction was found to be smaller due to the edge effect at the groove since the axial gage was placed near the groove step.

The large strain values recorded at the groove surface indicate that stresses are mostly concentrated in that region. During the shrink fitting process, stress induced failure is therefore expected to occur at that surface, especially in regions where curvature exists.

Stress relaxation due to cutting of the ring was also determined in this study. The gage readings just prior to critical failure were given in Table 8. The cut line was between TAN1 and TAN2. All three sets of strain values decreased during the curing process, with large contraction registered by TAN1 and TAN2 and small expansion by the AXIAL gage. This different extent of relaxation is expected since the cut was made in the close vicinity of the former two.

Table 8. Results for Rings with Outer Grooves

Ring-Shaft Materials		AL-AL	AL-SS
Tolerance		0.005"	0.005"
As-Fitted	CAL:	2660	3830
	TAN1:	420	599
	TAN2:	4066	3612
	AXI:	-647	-740
Prior to Failure	TAN1:	-424	-500
	TAN2:	-650	1200
	AXI:	-285	-410
After Ring Failure	TAN1:	-184	-168
	TAN2:	954	553
	AXI:	61	56

*All values in this table are in microstrains.

Rings with Inner Groove: A total of four assemblies were tested under this geometry. The geometry and the locations of the three strain gages are given in Figure 26c. It is important to note here that the two tangential gages (TAN1 and TAN2) were located on the outer surface and the inner groove, respectively. Results from this series of tests are given in Table 9. In the as-fitted condition, the TAN1 reading for the Al-SS assembly is extremely low. This low reading is most likely due to the loosening of the gage on the sample during the experiment. It is evident that the strains and therefore the stresses at TAN2 (the inner groove surface) are extremely high and rather consistent. These values (7000 to 8000 microstrain) are about twice as expected from the theoretical hoop strain calculation (nominally below 3000 microstrain). It is critical to realize that in this inner groove configuration, the groove portion of the ring is not in contact with the shaft and therefore it does not experience the radial stress from the fitting process. The calculated values in Table 9 are obtained based on the following phenomenon. It is reasonable to visualize that shrink fitting forces the ring radially outward at the region of contact (not the groove). This outward motion introduces a hoop tensile stress at the grooves which possess the smallest cross sectional area. An overall outward motion of 0.005" (radially results in an increase of the circumference by 0.016". When this elongation is accommodated by the four grooves (each of 0.5" in width), it produces an effective strain of 7,854 microstrain. This calculated strain agrees very well with the measured values of 7,146 and 8,215 microstrains. Preliminary finite element analysis based on ANSYS shows that the highest tangential stress occurs at the middle of the inner groove with a strain of 6600 microstrain. This ANSYS value is higher than the similar value for the outer

groove in agreement with the measurements.

The very large strains at the inner groove region of this configuration (the highest observed in this experiment), indicate that failure will mostly occur at the bottom of the inner groove in such a configuration. It is therefore critical to eliminate any curvature in that surface which may lead to stress concentrations.

Strain relaxation experiments were also conducted in these samples with the cut being made between TAN1 and TAN2. Relaxation of the fitting induced strain was observed in the TAN1 and AXI gages as illustrated in Table 9. However, the reading at TAN2 increased due to cutting reaching maximum values of 10,825 and 11,560 microstrain, respectively, for Al-Al and Al-SS assemblies just prior to critical failure. These values then decreased by 50% upon failure. It is because the cutting process does not constitute a source of stress. It is probable that the increase in the strain in TAN2 during cutting is the result of the shape change at the region of the groove. The initial shrink fitting process leads to a circular expansion of the ring, including the groove region. During the cutting process, the curvature of the groove region relaxes resulting in a bending motion which expands the inside surface where TAN2 is located.

As a result of this portion of the investigation, we have determined the feasibility of employing strain gages to determine the strain (and therefore stress) induced by the shrink fitting process was demonstrated. It is evident from the data obtained in this preliminary work that more precise determination of the stress distribution can be obtained if more strain gages are used. Nevertheless the strategic placing of three gages is sufficient to

Table 9. Results for Rings with Outer Grooves

Ring-Shaft Materials Tolerance		AL-AL 0.005"	AL-SS 0.005"
As-Fitted	CAL:	7854	7854
	TAN1:	3344	229
	TAN2:	7146	8215
	AXI:	-911	-883
Prior to Failure	TAN1:	600	-1413
	TAN2:	10825	11560
	AXI:	-323	-414
After Ring Failure	TAN1:	96	-703
	TAN2:	4871	5620
	AXI:	-70	-78

*All values in this table are in microstrains.

yield valuable information on the stress state at critical locations. Results from the ring with a uniform cross section indicate the validity of simple stress mechanics calculation for determining the stress state induced in this geometry by shrink fitting. For a ring with an outer groove geometry, much of the stress was found to be at the groove surface. The stress level at that surface appears to correspond to a simple ring with a thickness equal to the thinnest portion of the groove. A high stress state was found in a ring with an inner groove at the inner surface of the groove. In this case, the stress state can be approximated by a tensile stress with the entire strain being accommodated by the groove region. The Strain relaxation due to curing provided information on the deformation of the ring during the cutting process.

e. The analysis of shrink fitting stress using finite element. A finite element analysis program based on ANSYS was developed to calculate the stress

distribution generated by shrink fitting. This program was used to calculate the stress distributions in two different geometries: plain cross section, and roller bearing. The Sun network operated by the College of Engineering at Auburn was used for these calculations. Results for the plain cross section are given in figures 27 and 28. In this case, the ID of the ring was forced to be displaced outward by 0.005" (assumed to be generated by the shrink fitting misfit). Figure 27 illustrates the stress in the x direction where x is along the horizontal. The dark tone represents tensile while the light tone represents compression as indicated in the scale on the right hand size. Since this is a plot of the stress along the x-direction, the stress state at the top of the figure is hoop in nature whereas the stress state at the right hand side of the figure is radial in nature. In the middle, the stress state is in shear. Figure 27 shows that the inner surface experiences a high tensile stress of about 60 ksi (see the dark triangle near the top of the figure) whereas the radial stress is very low. This high tensile stress at the inner surface suggests that failure due to shrink fitting would initiate from the ID outward in accord with observation. Figure 28 shows the σ_{xy} for the sample stress condition. As expected, the distribution possesses a two fold symmetry due to the x-y orthogonal geometry used.

Figures 29 and 30 show the stress distribution in an inner race configuration. Figure 29 gives the radial stress as a function of radial position whereas figure 30 gives the hoop (or tangential stress). In these calculations, a uniform outward stress of 30 ksi was application on the ID of the ring. As illustrated in figure 29, the radial stress at the ID is 30 ksi in compression and this radial stress decay to zero at the outside surface. The outside surface must maintain a zero normal stress since it is a free

surface. Figure 30 shows that there exists a high tensile stress (160 ksi) in the hoop direction at the inner surface near the smaller step. This high tensile stress state is believed to be responsible for crack initiation during the shrink fitting process. This analysis indicates that the highest tensile stress in the system occurs at the ID of the ring with a stress value of over 5 times that of the applied radial stress.

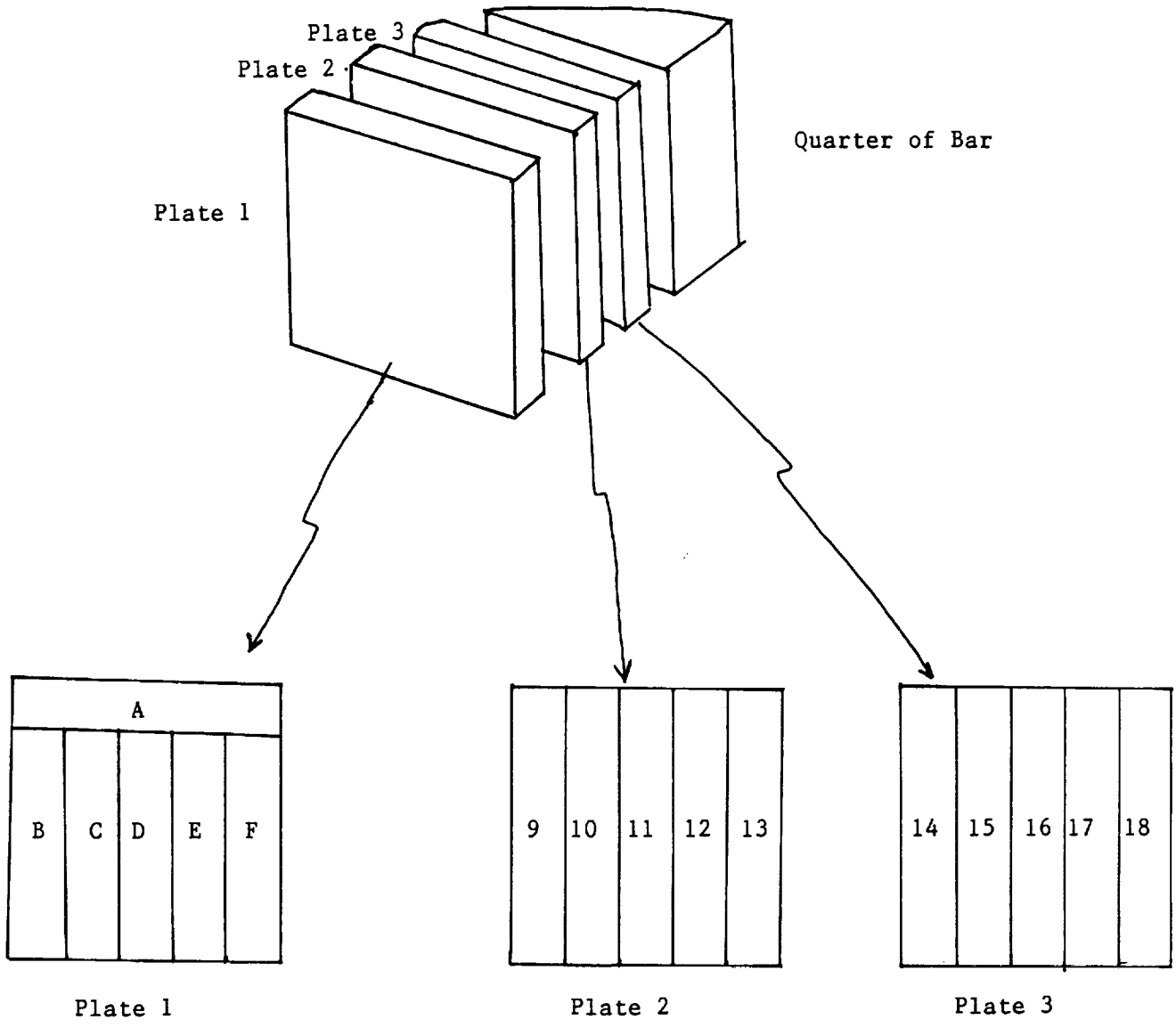

Figure 1. Locations of the specimens in Group A used in mechanical testing.

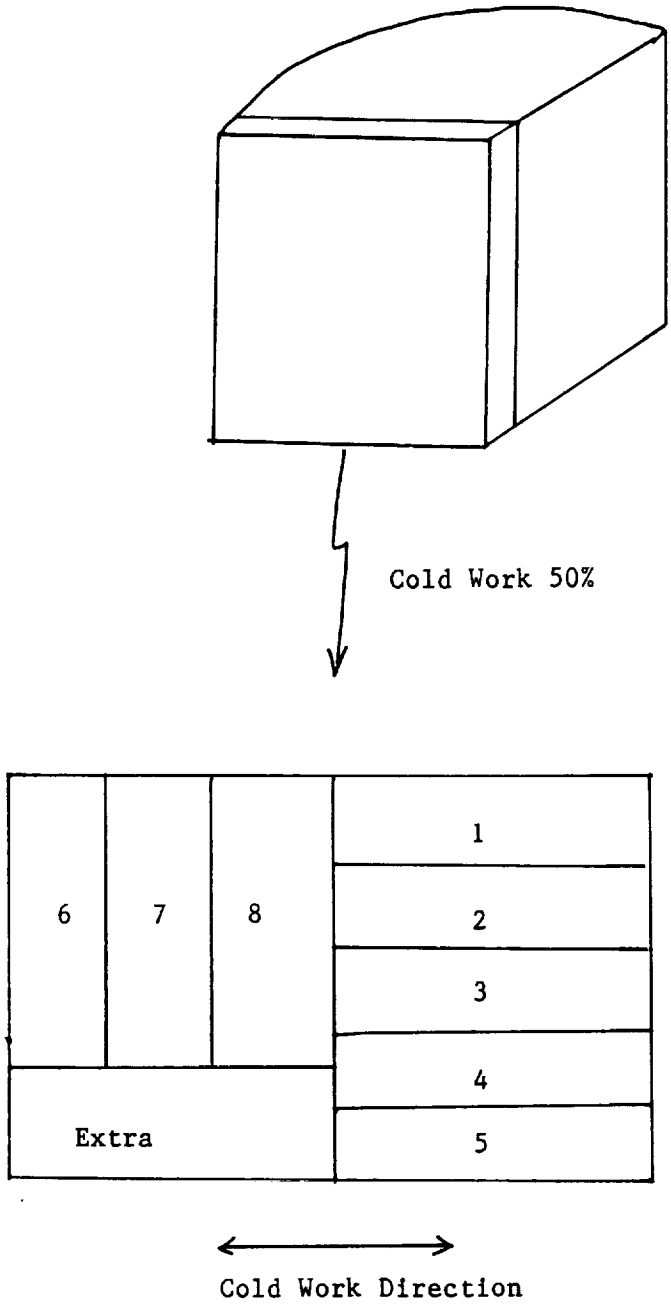

Figure 2. Locations of the specimens in Group B used in mechanical testing.

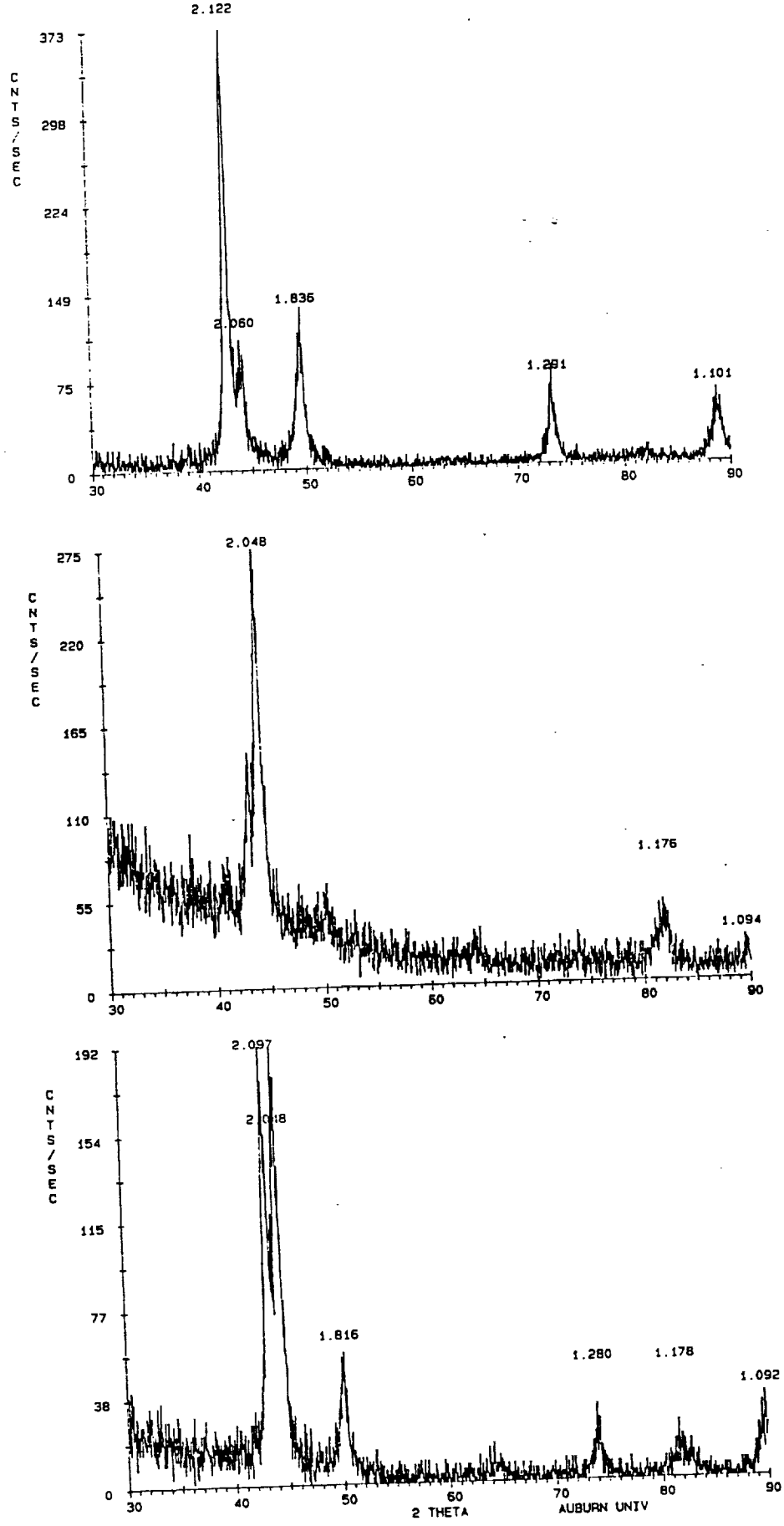

Figure 3. Diffraction patterns from specimen A taken from the longitudinal, long transverse and short transverse directions.

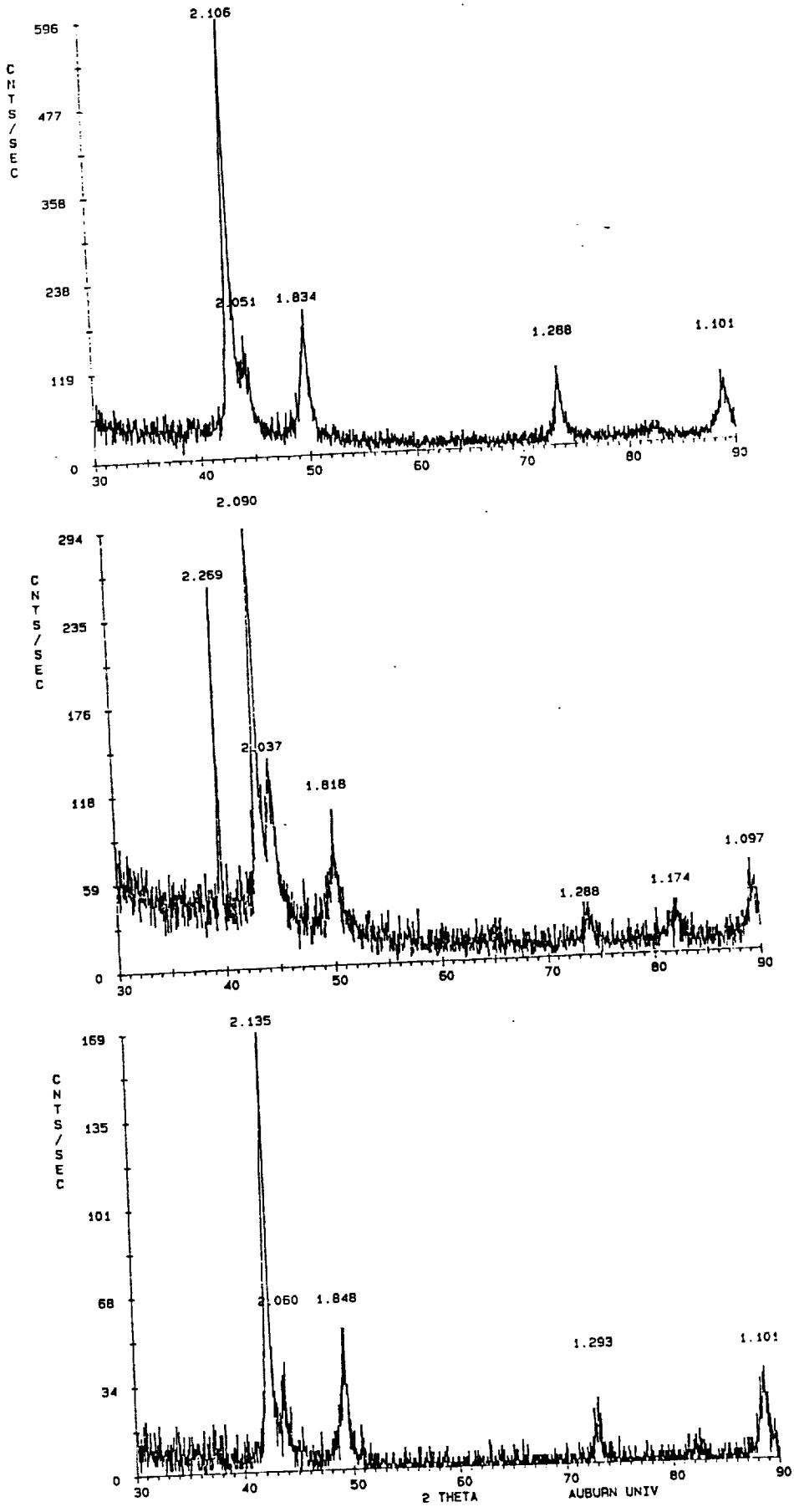

Figure 4. Diffraction patterns from specimen B taken from the longitudinal, long transverse and short transverse directions.

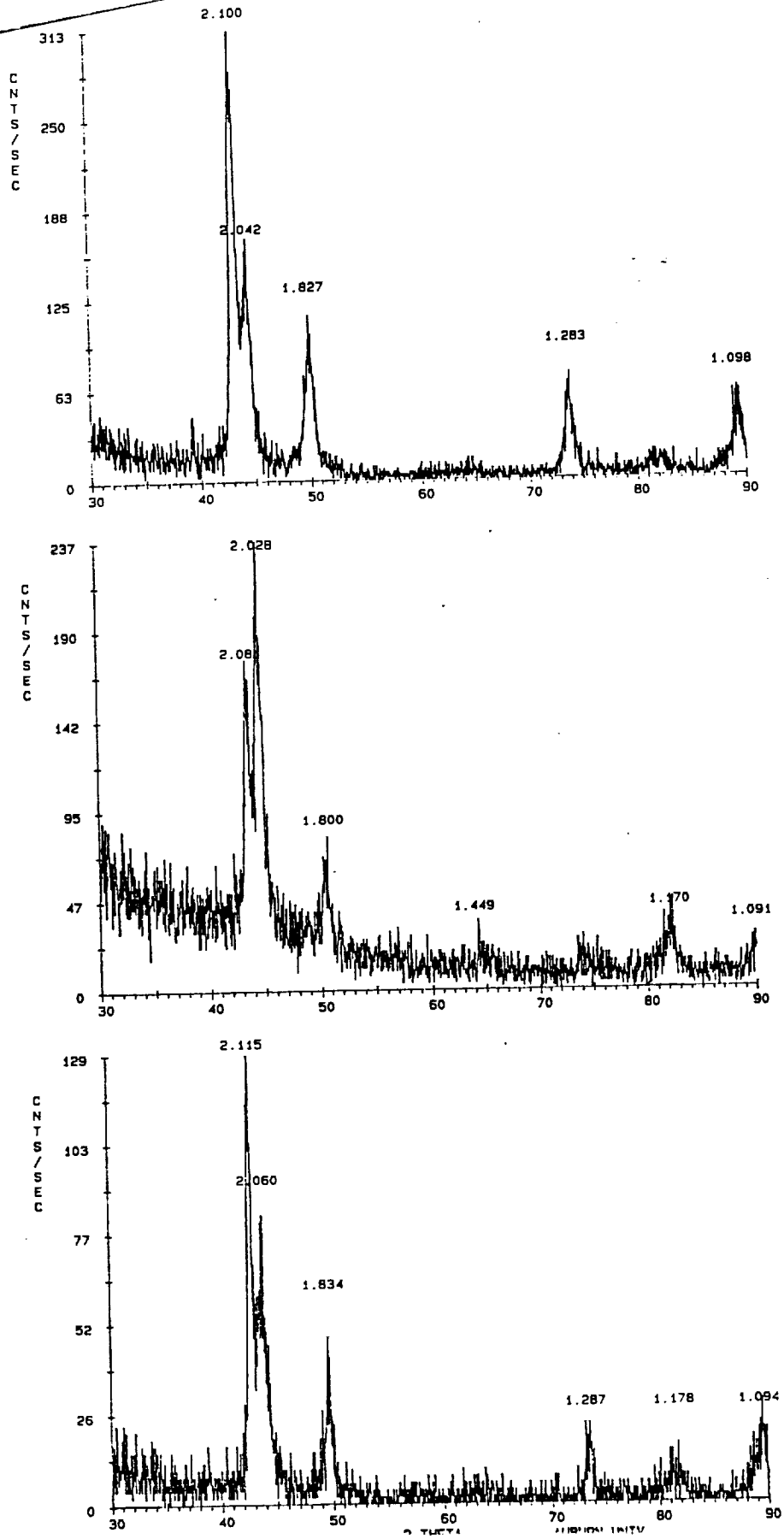

Figure 5. Diffraction patterns from specimen C taken from the longitudinal, long transverse and short transverse directions.

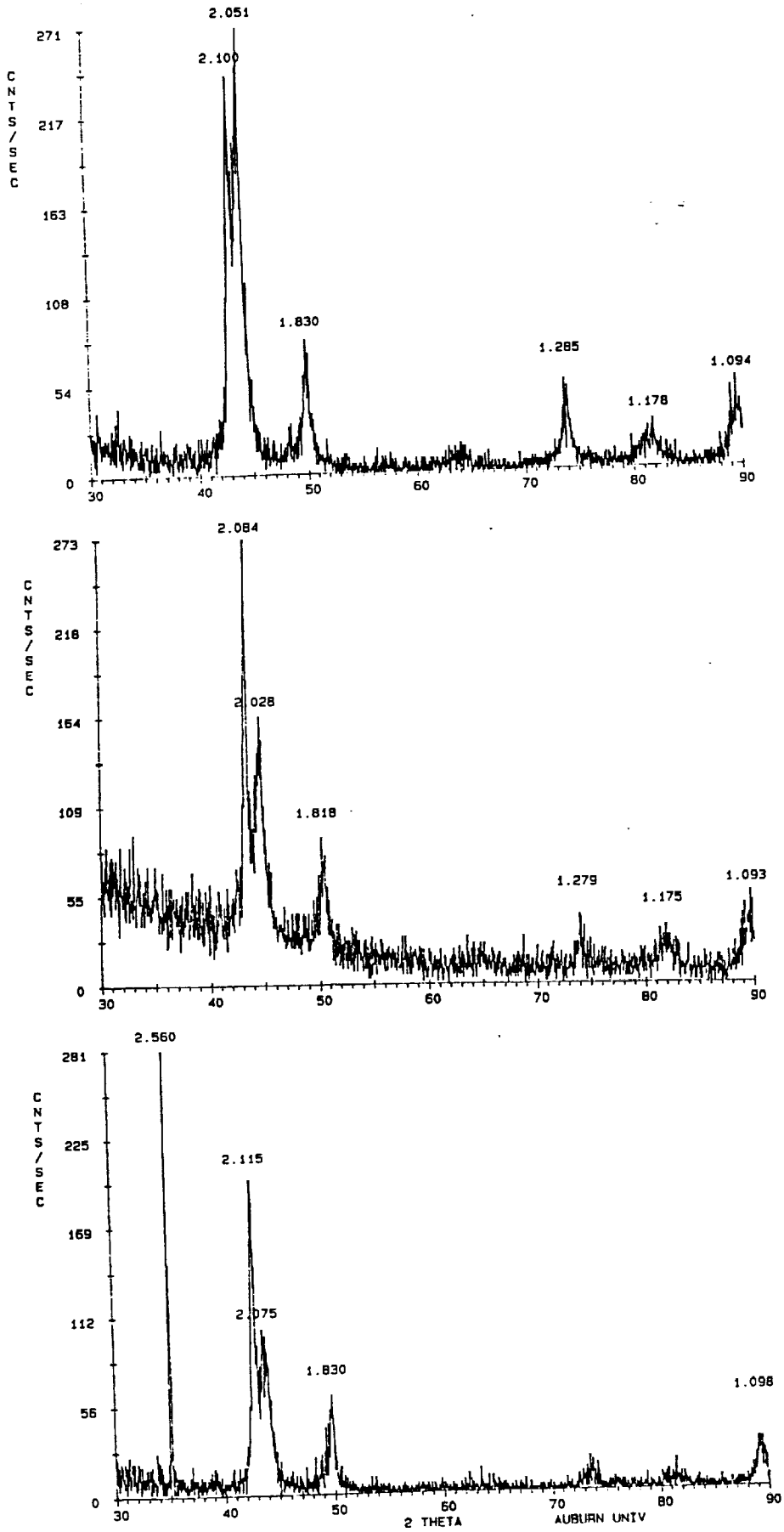

Figure 6. Diffraction patterns from specimen E taken from the longitudinal, long transverse and short transverse directions.

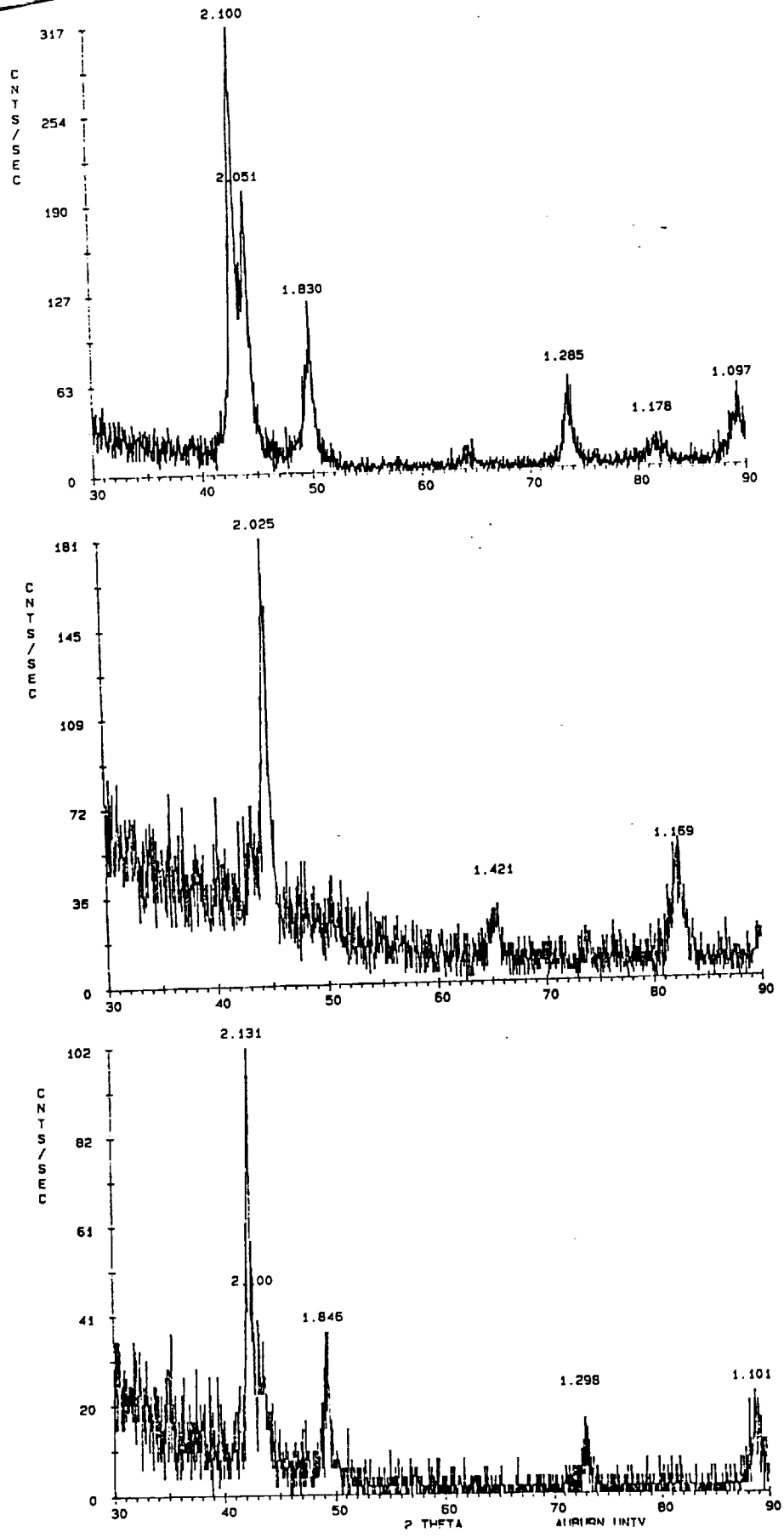

Figure 7. Diffraction patterns from specimen F taken from the longitudinal, long transverse and short transverse directions.

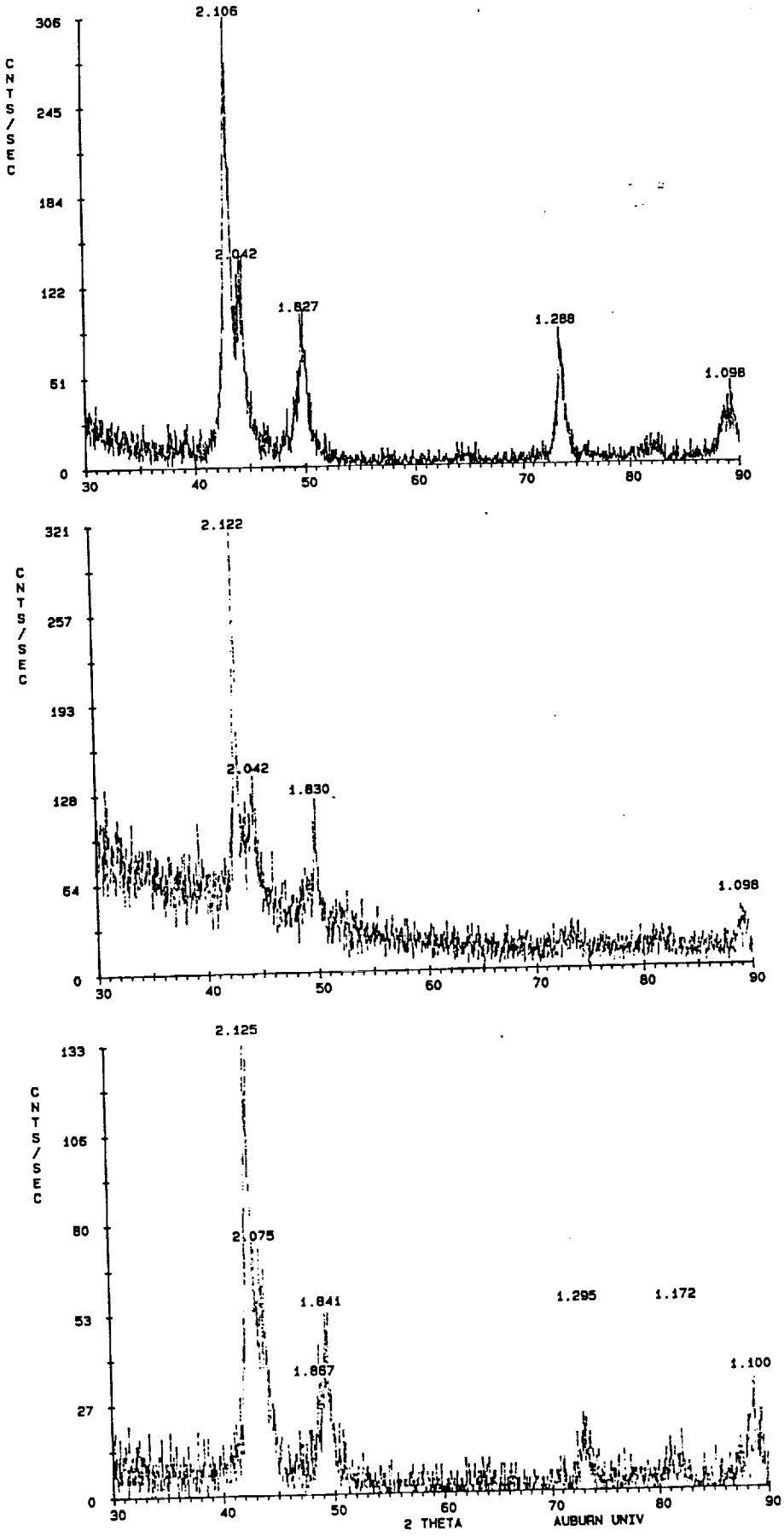

Figure 8. Diffraction patterns from specimen 1 taken from the longitudinal, long transverse and short transverse directions.

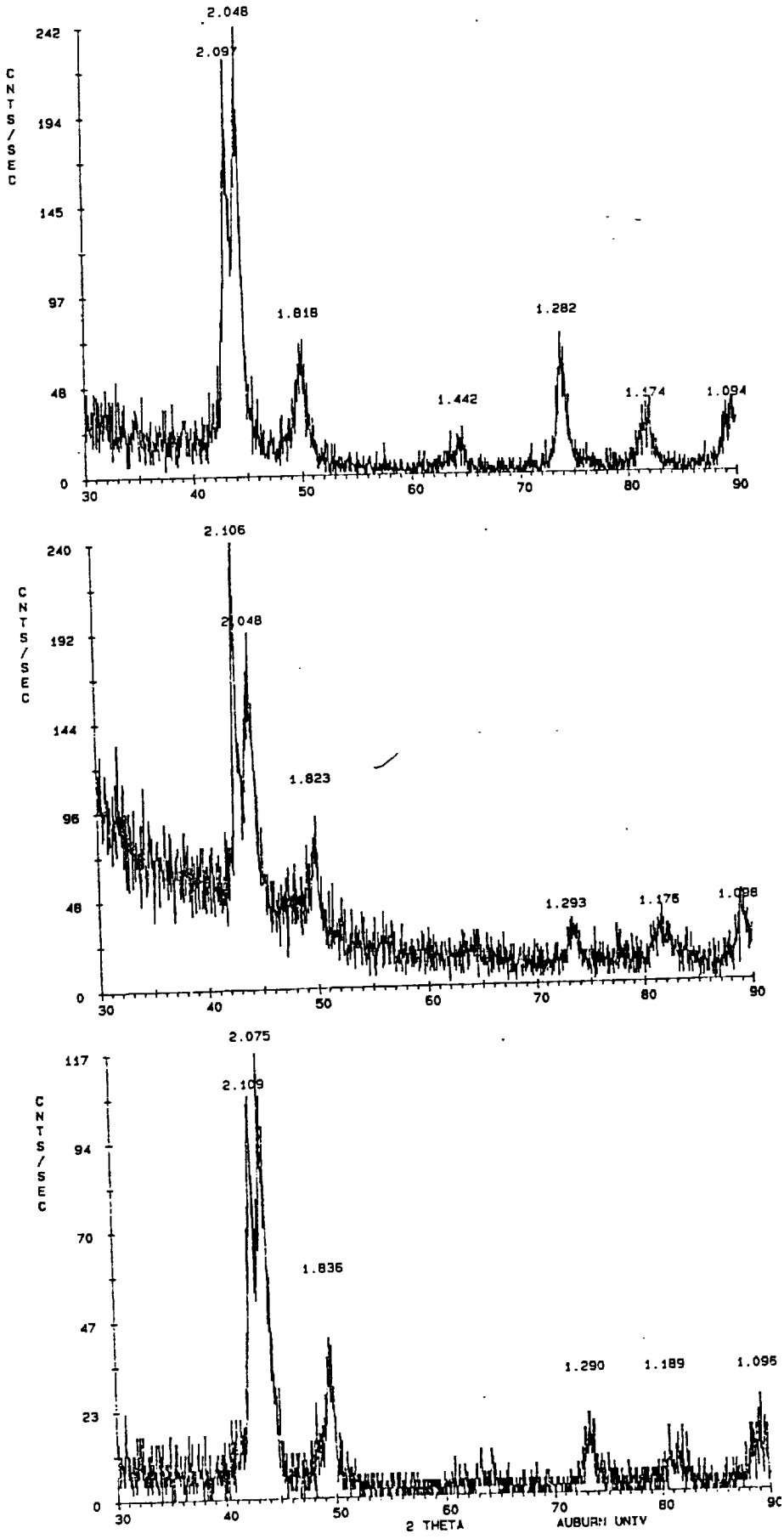

Figure 9. Diffraction patterns from specimen 2 taken from the longitudinal, long transverse and short transverse directions.

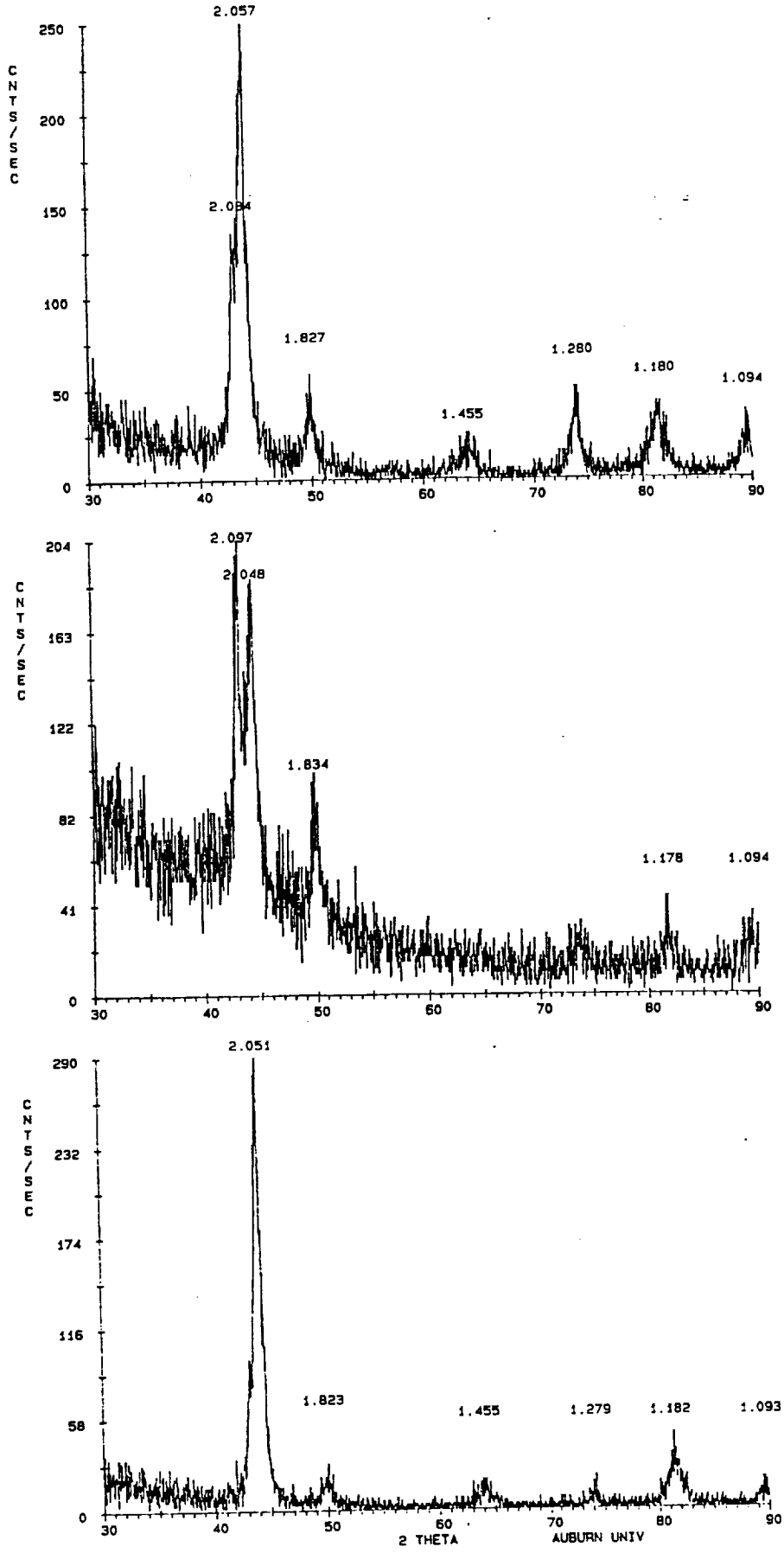

Figure 10. Diffraction patterns from specimen 3 taken from the longitudinal, long transverse and short transverse directions.

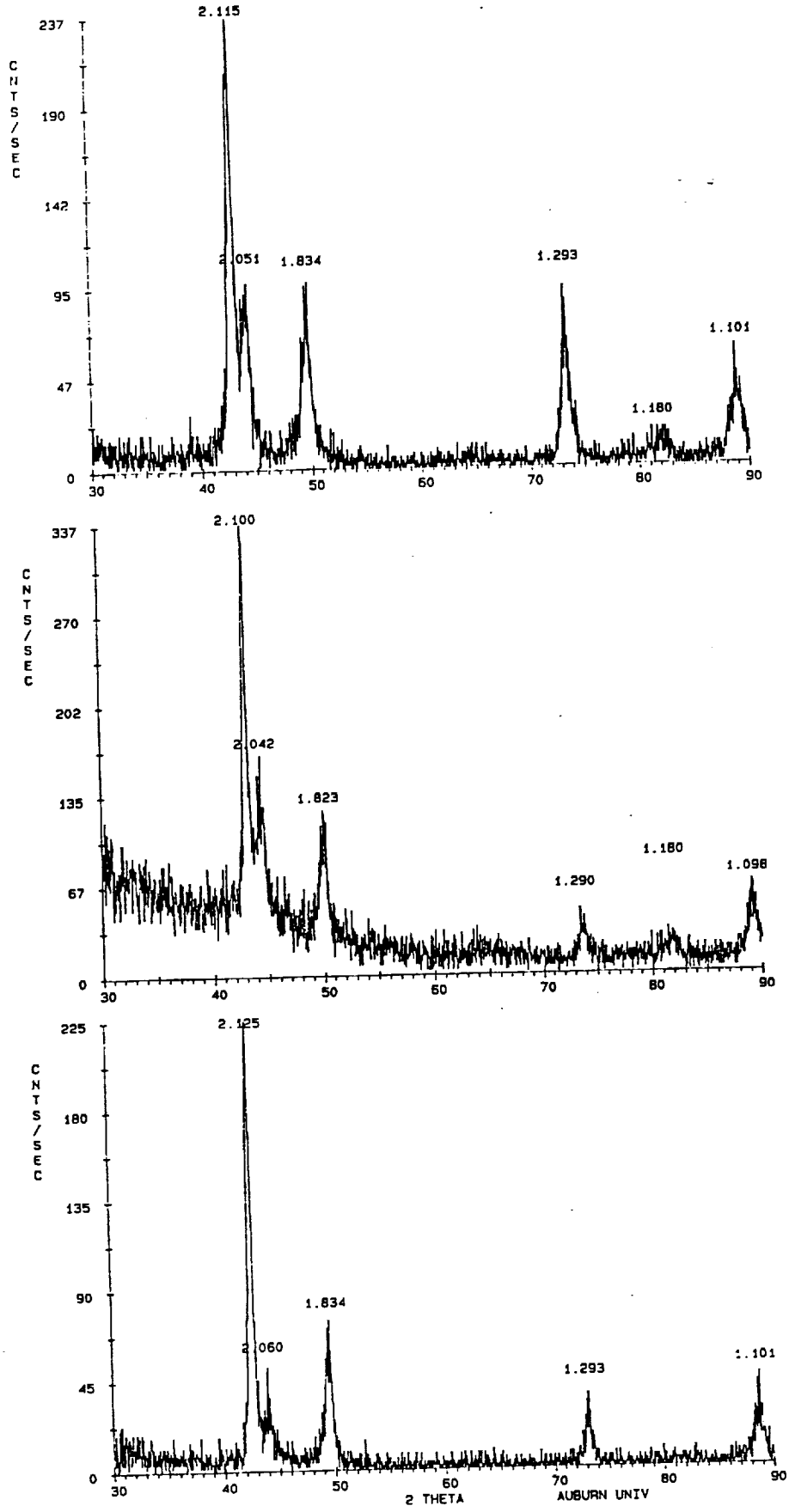

Figure 11. Diffraction patterns from specimen 4 taken from the longitudinal, long transverse and short transverse directions.

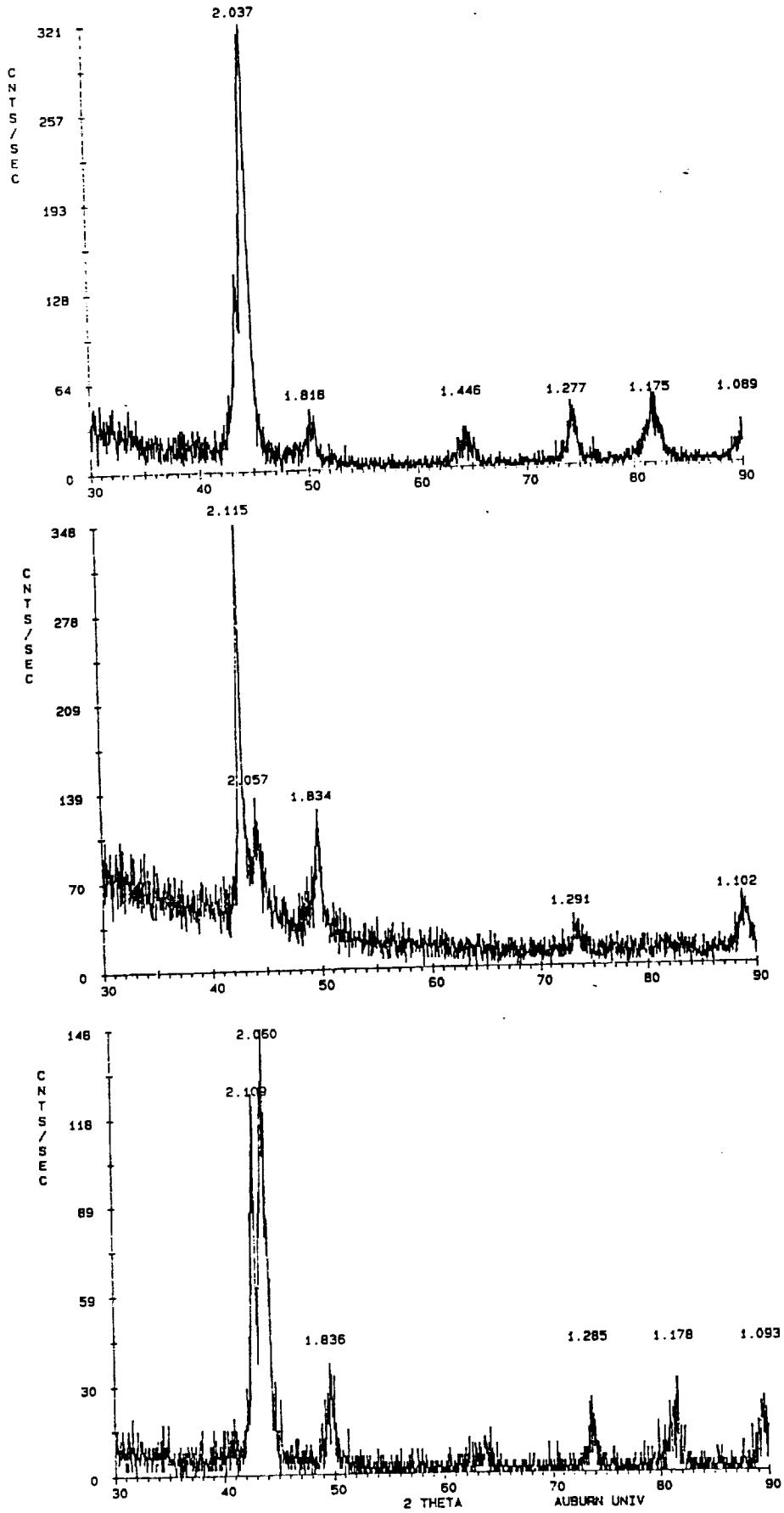

Figure 12. Diffraction patterns from specimen 5 taken from the longitudinal, long transverse and short transverse directions.

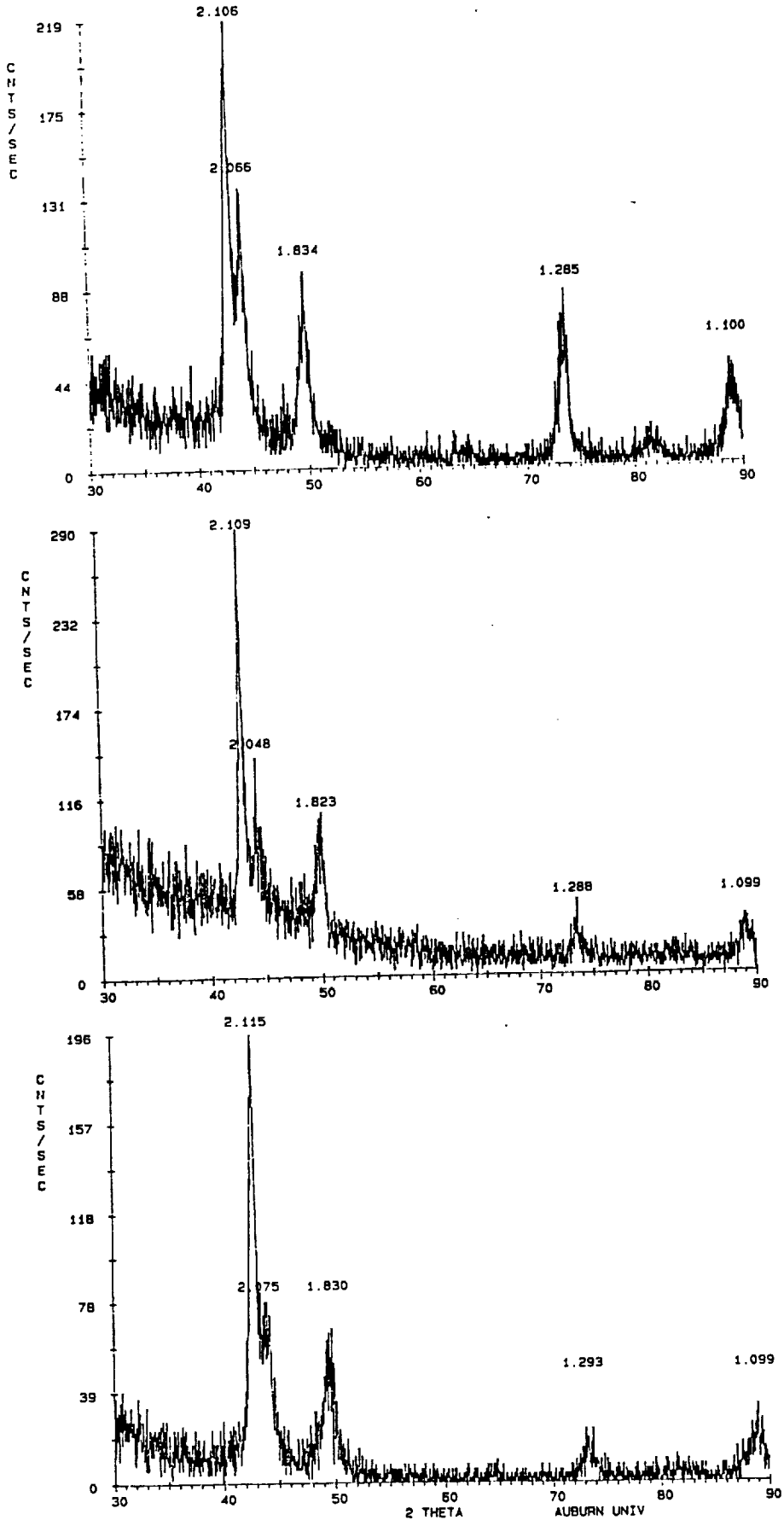

Figure 13. Diffraction patterns from specimen 6 taken from the longitudinal, long transverse and short transverse directions.

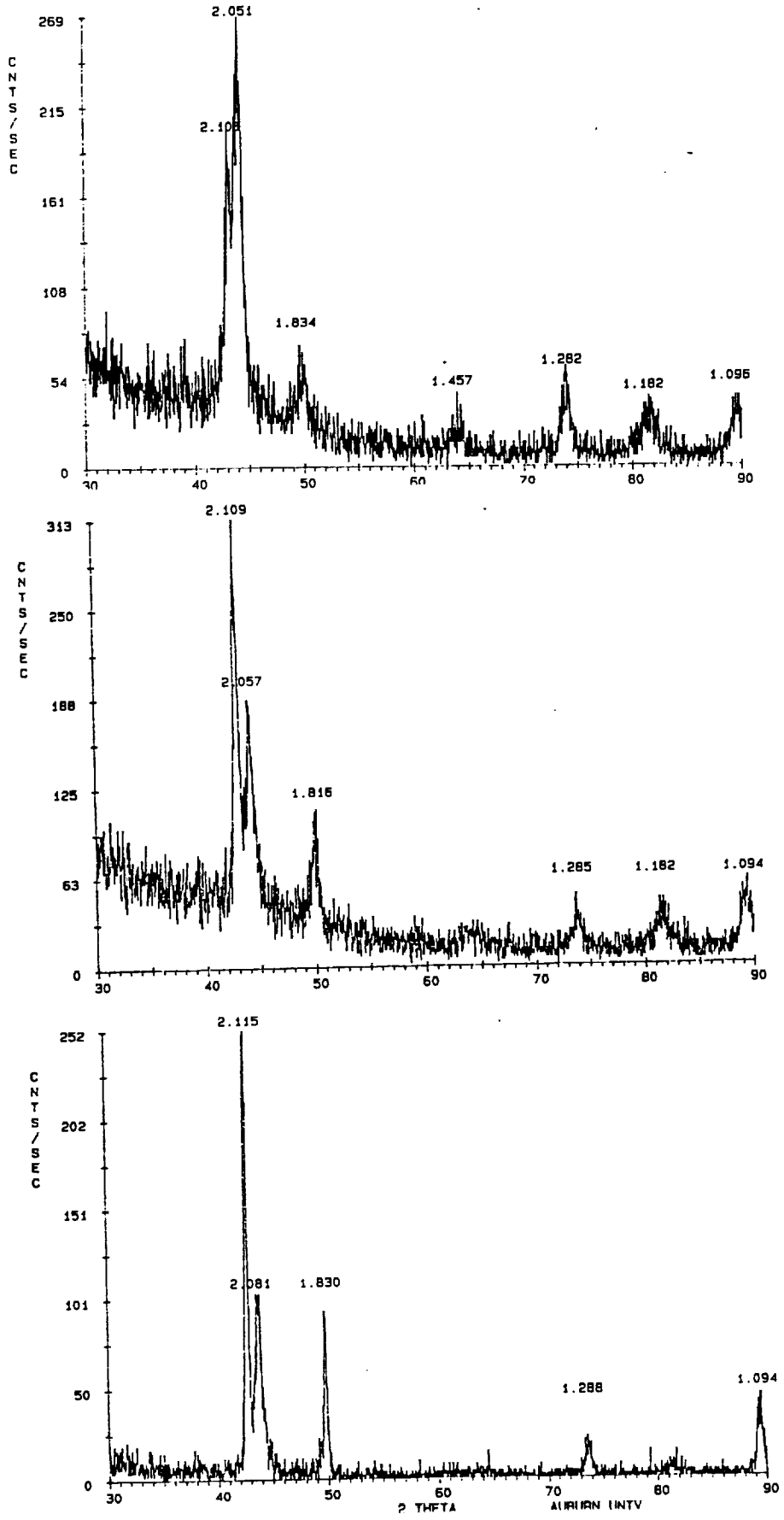

Figure 14. Diffraction patterns from specimen 7 taken from the longitudinal, long transverse and short transverse directions.

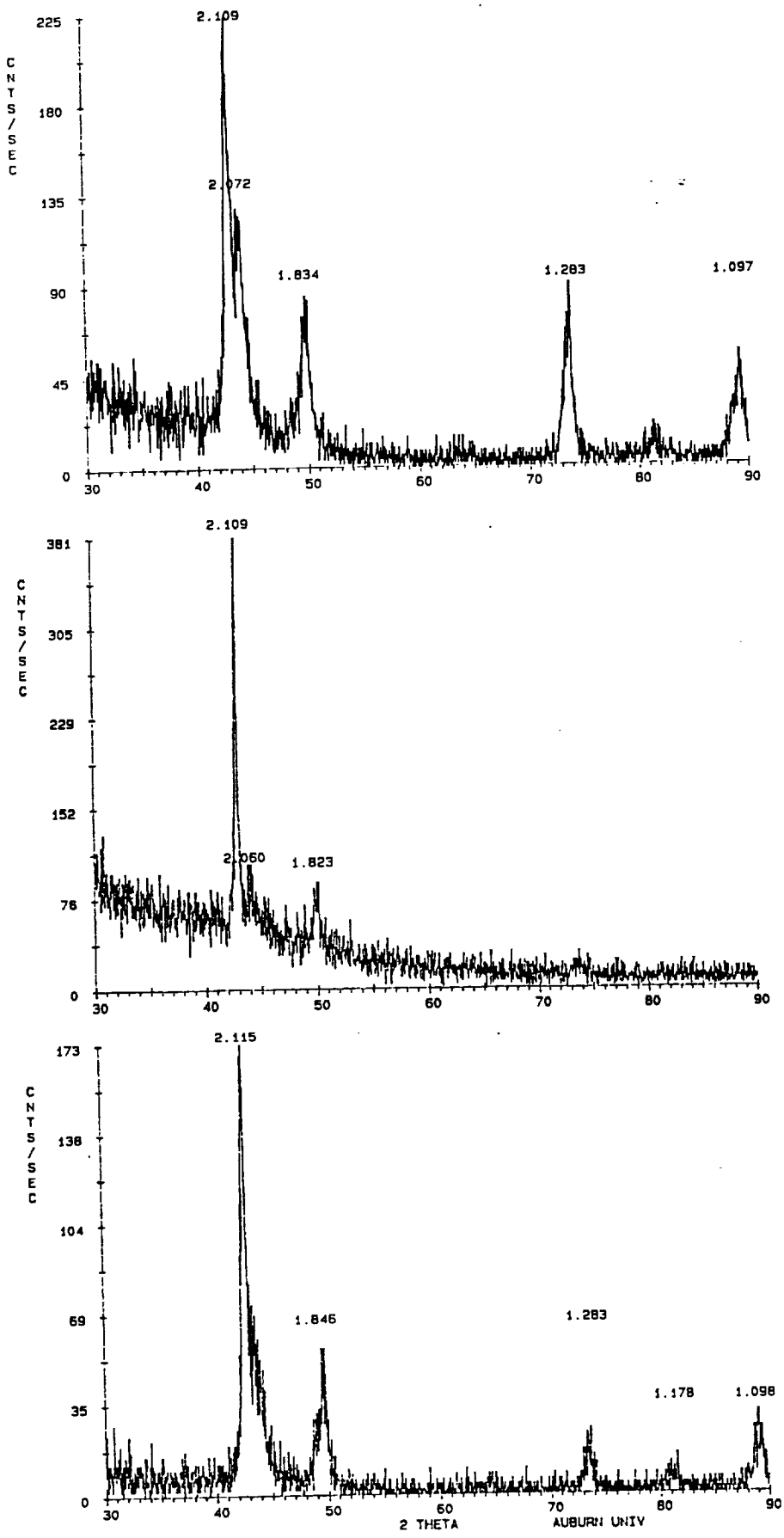

Figure 15. Diffraction patterns from specimen 8 taken from the longitudinal, long transverse and short transverse directions.

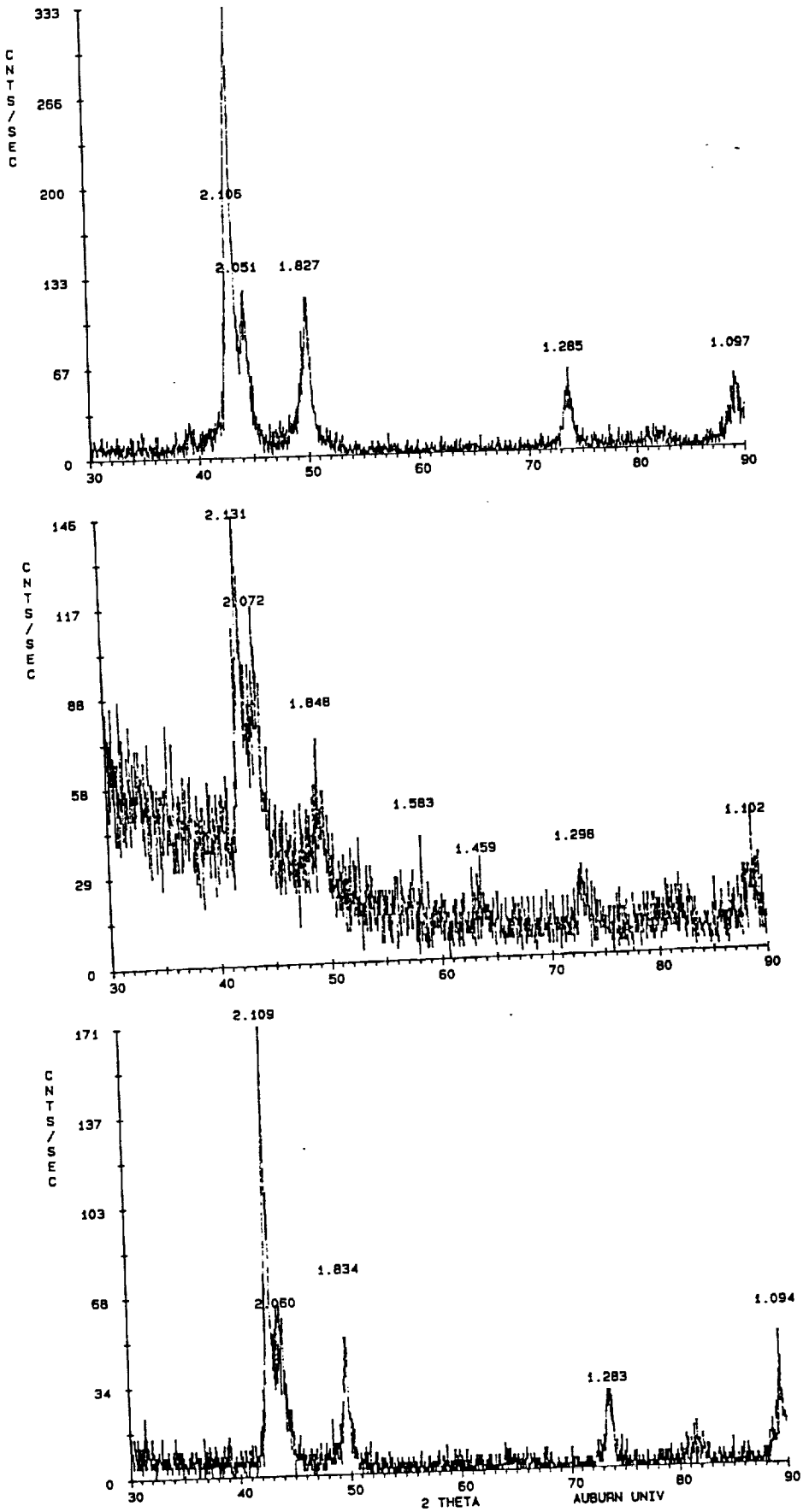

Figure 16. Diffraction patterns from specimen 9 taken from the longitudinal, long transverse and short transverse directions.

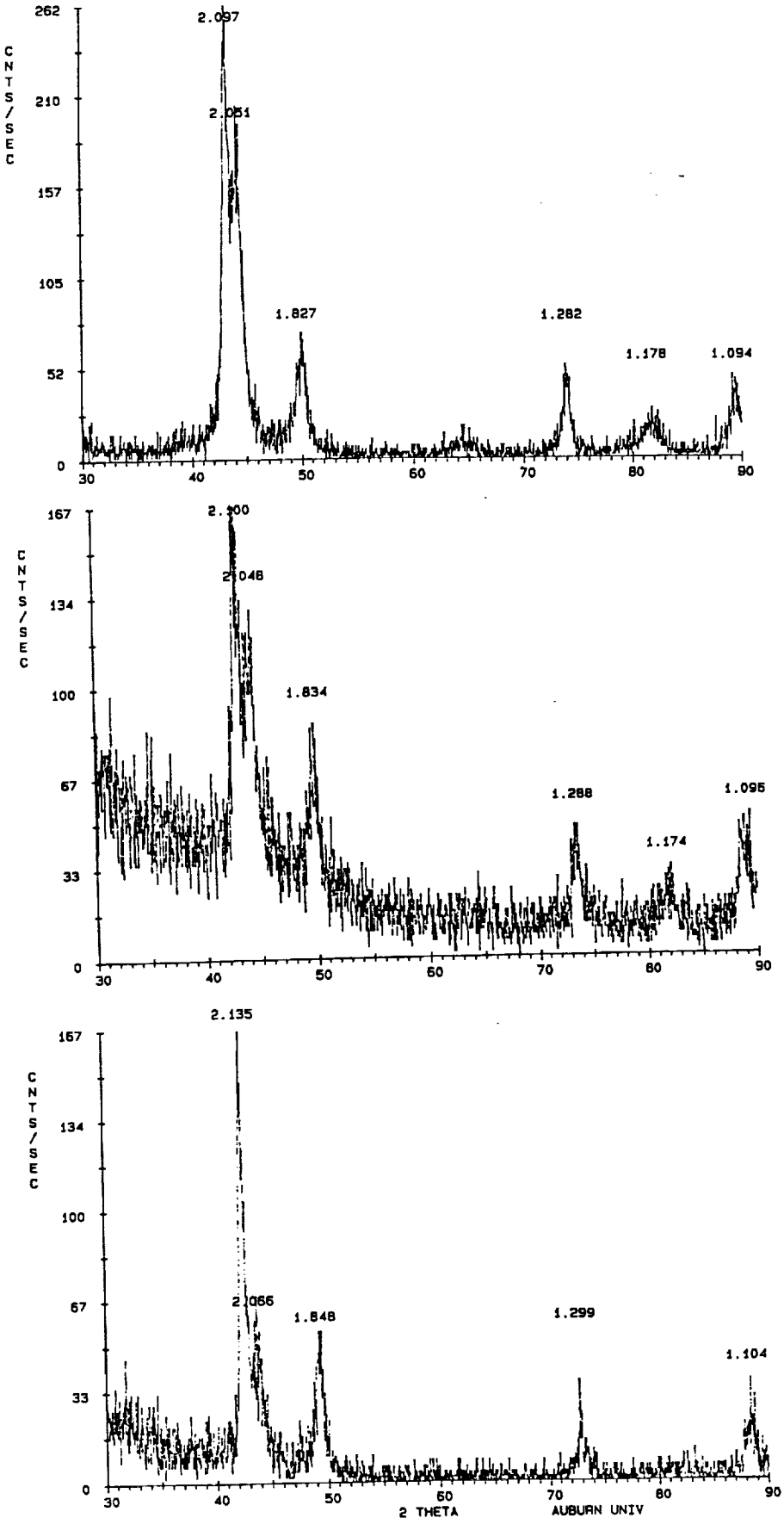

Figure 17. Diffraction patterns from specimen 10 taken from the longitudinal, long transverse and short transverse directions.

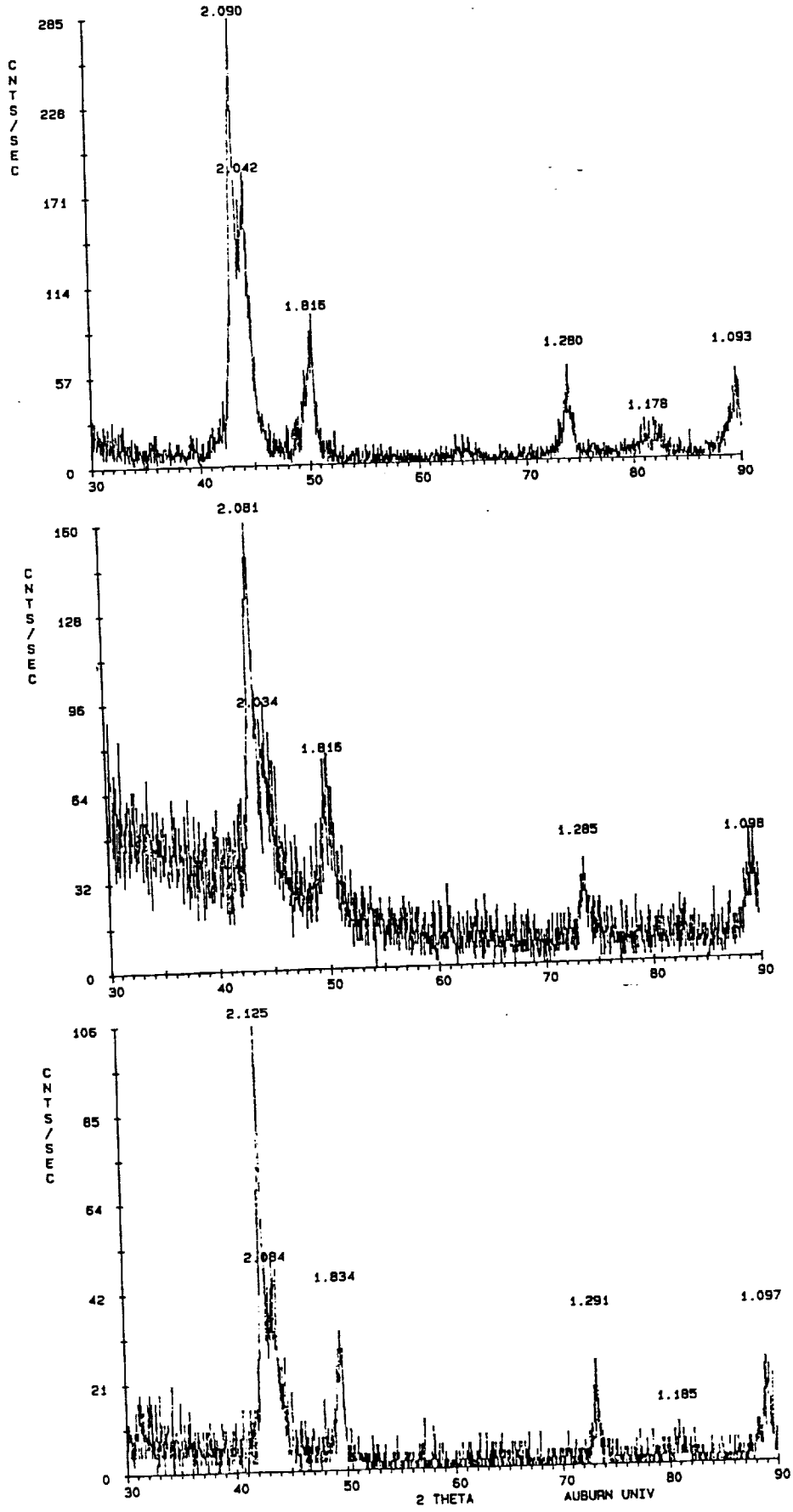

Figure 18. Diffraction patterns from specimen 11 taken from the longitudinal, long transverse and short transverse directions.

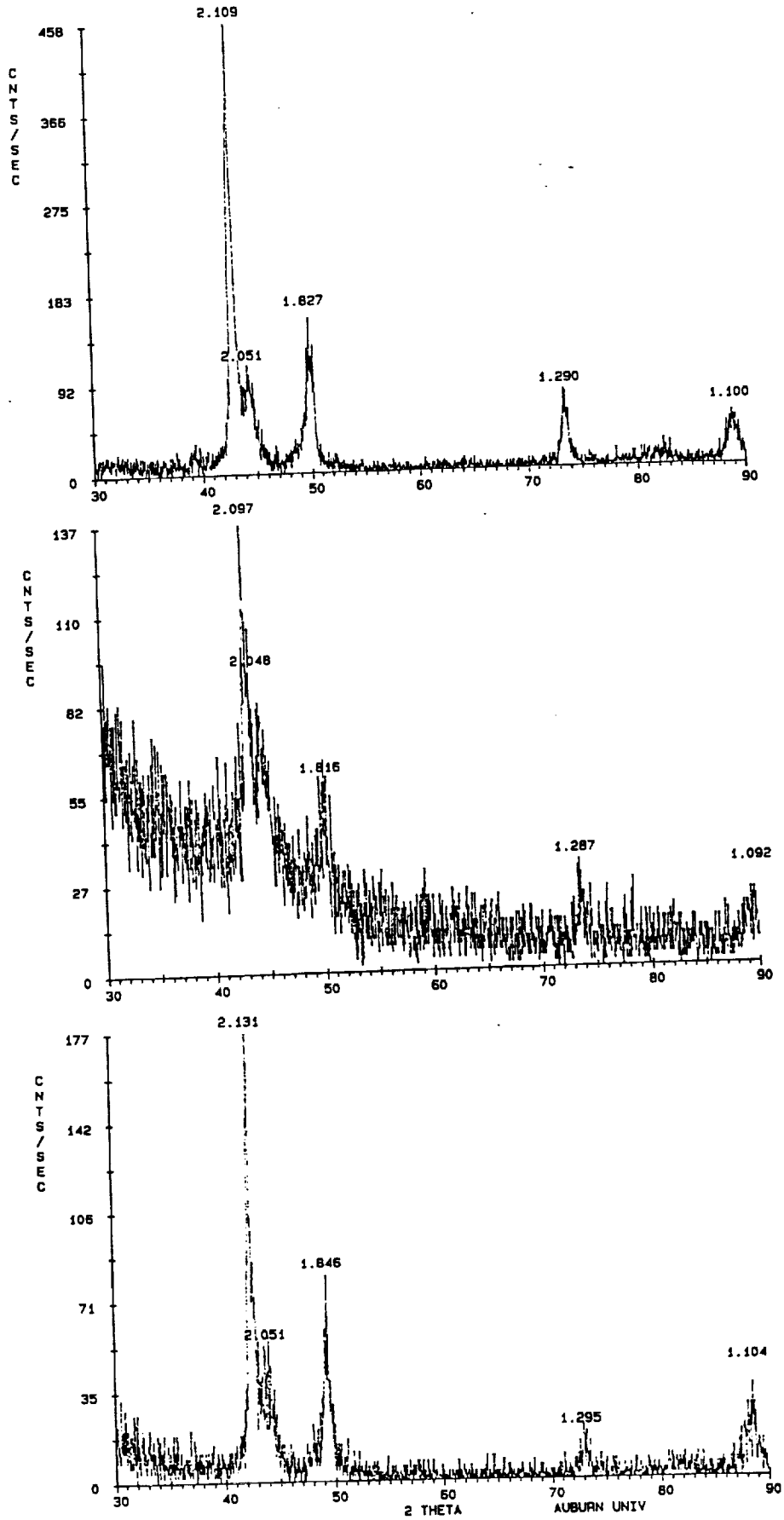

Figure 19. Diffraction patterns from specimen 12 taken from the longitudinal, long transverse and short transverse directions.

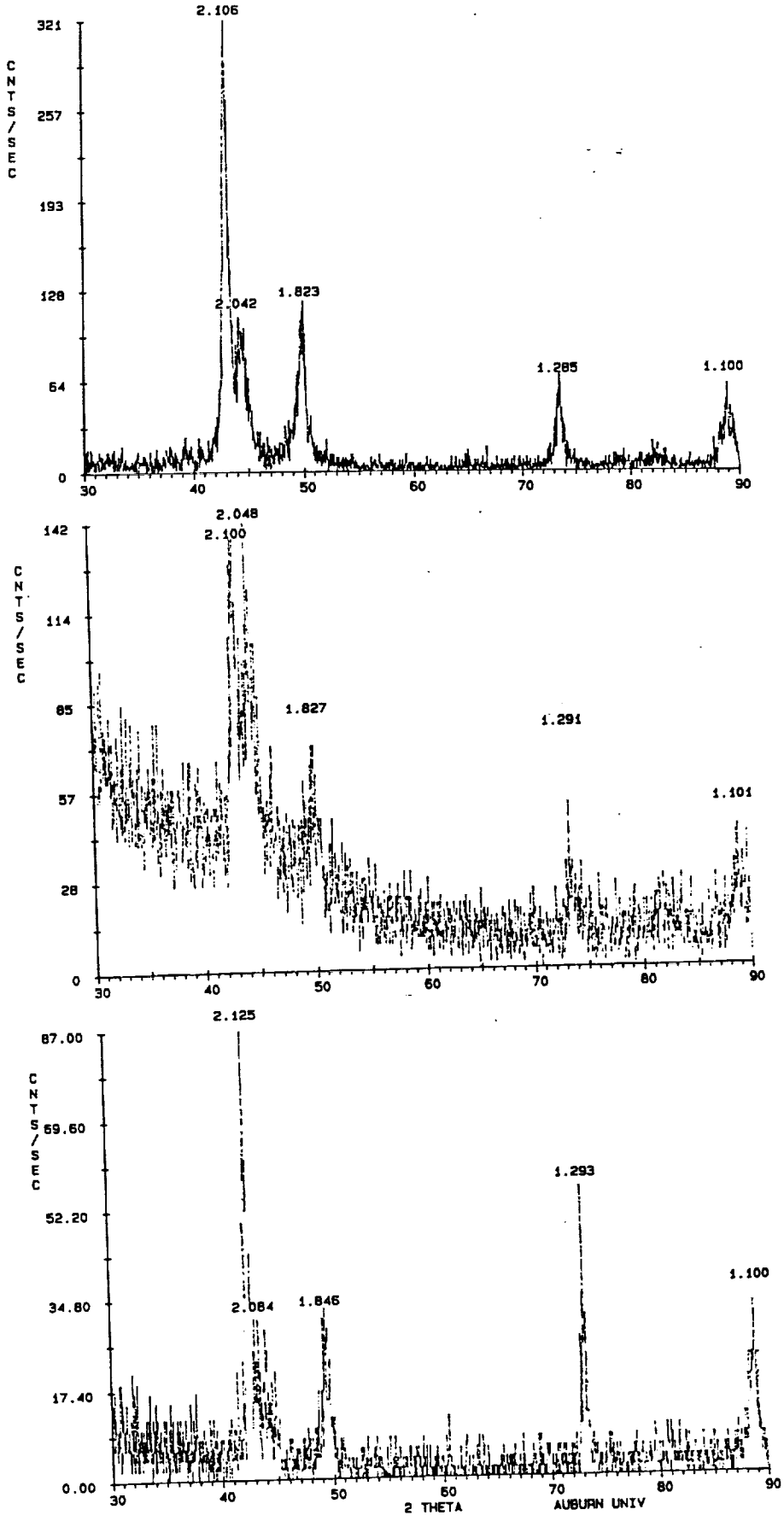

Figure 20. Diffraction patterns from specimen 13 taken from the longitudinal, long transverse and short transverse directions.

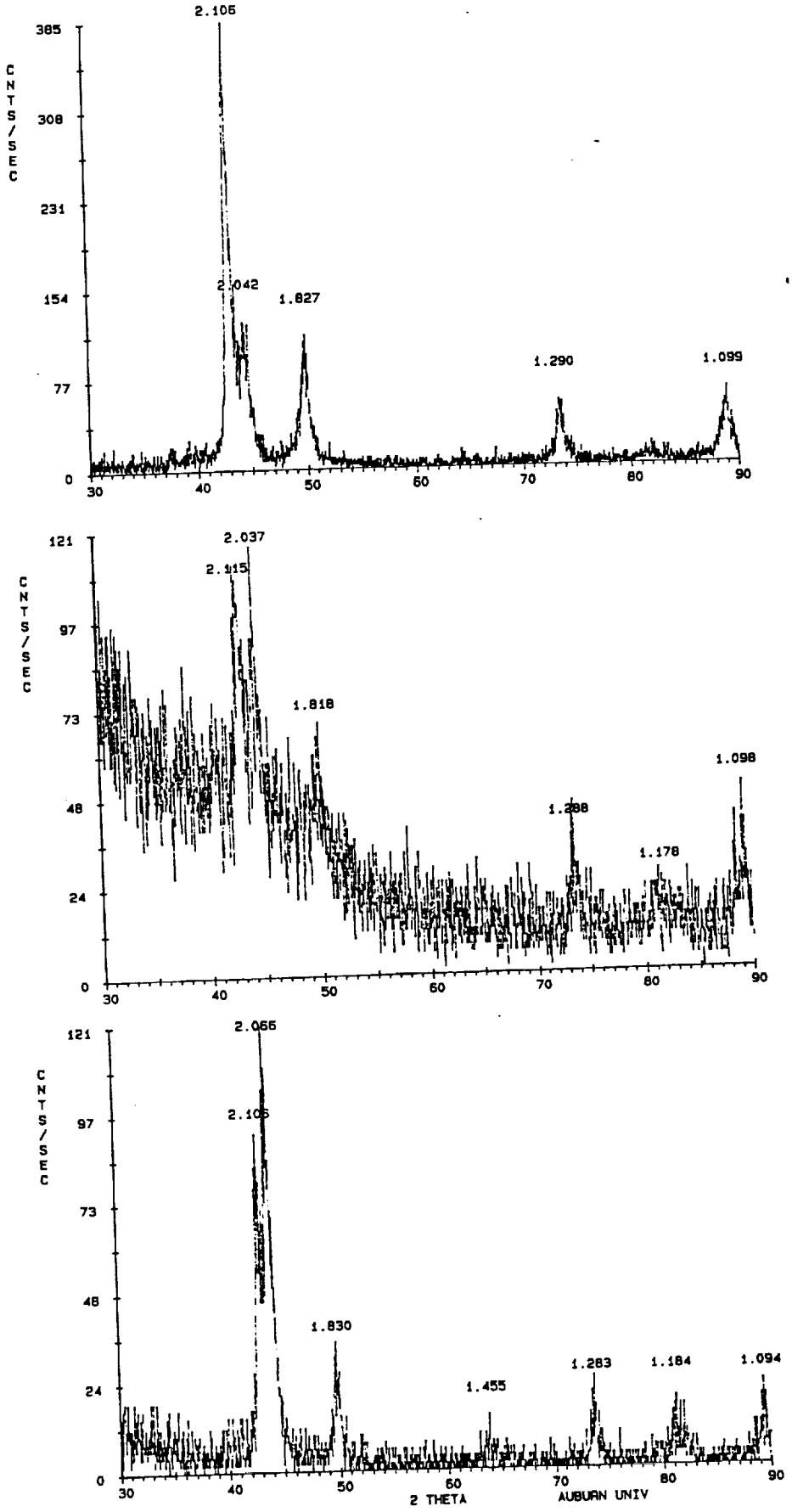

Figure 21. Diffraction patterns from specimen 14 taken from the longitudinal, long transverse and short transverse directions.

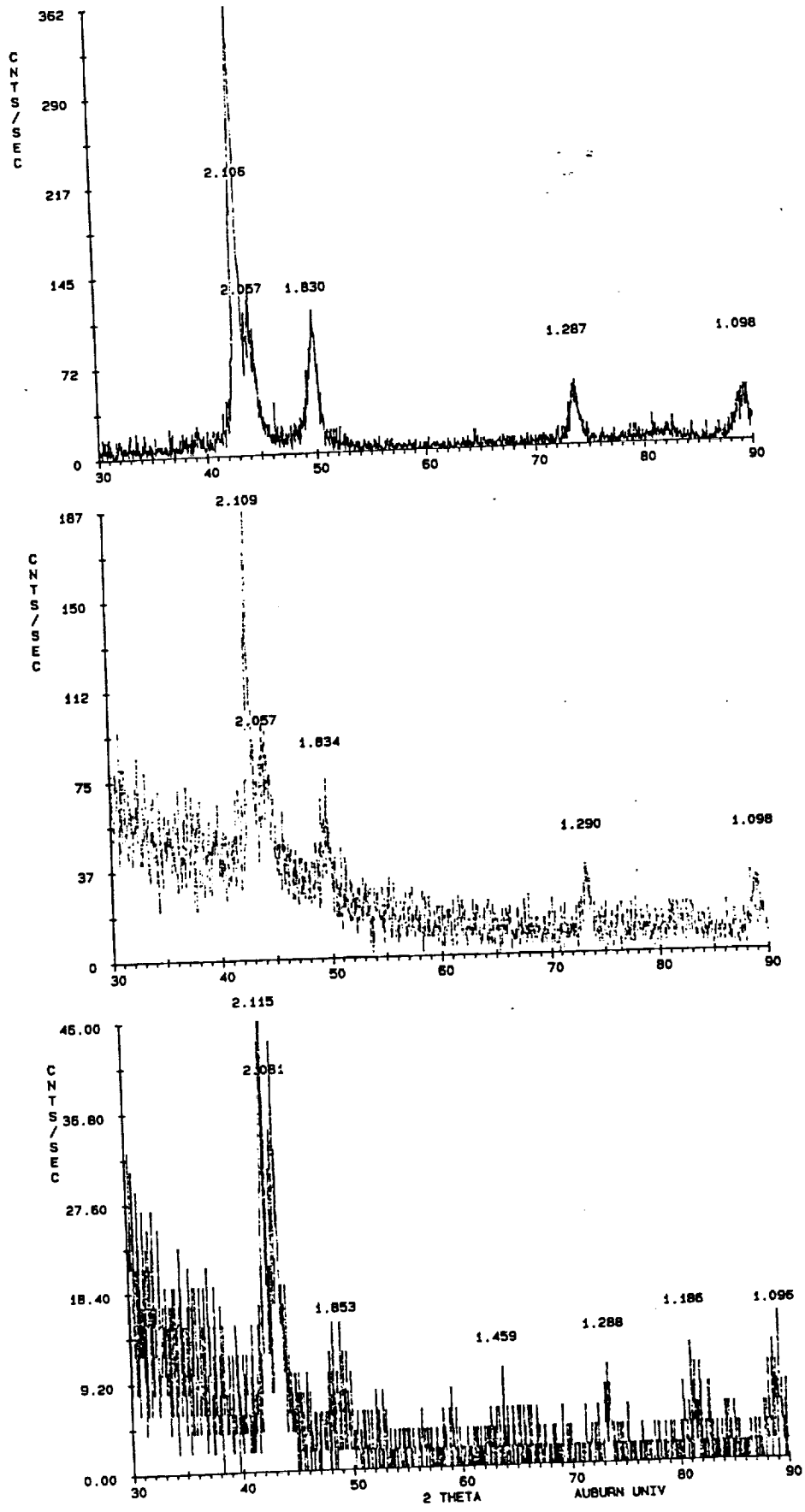

Figure 22. Diffraction patterns from specimen 15 taken from the longitudinal, long transverse and short transverse directions.

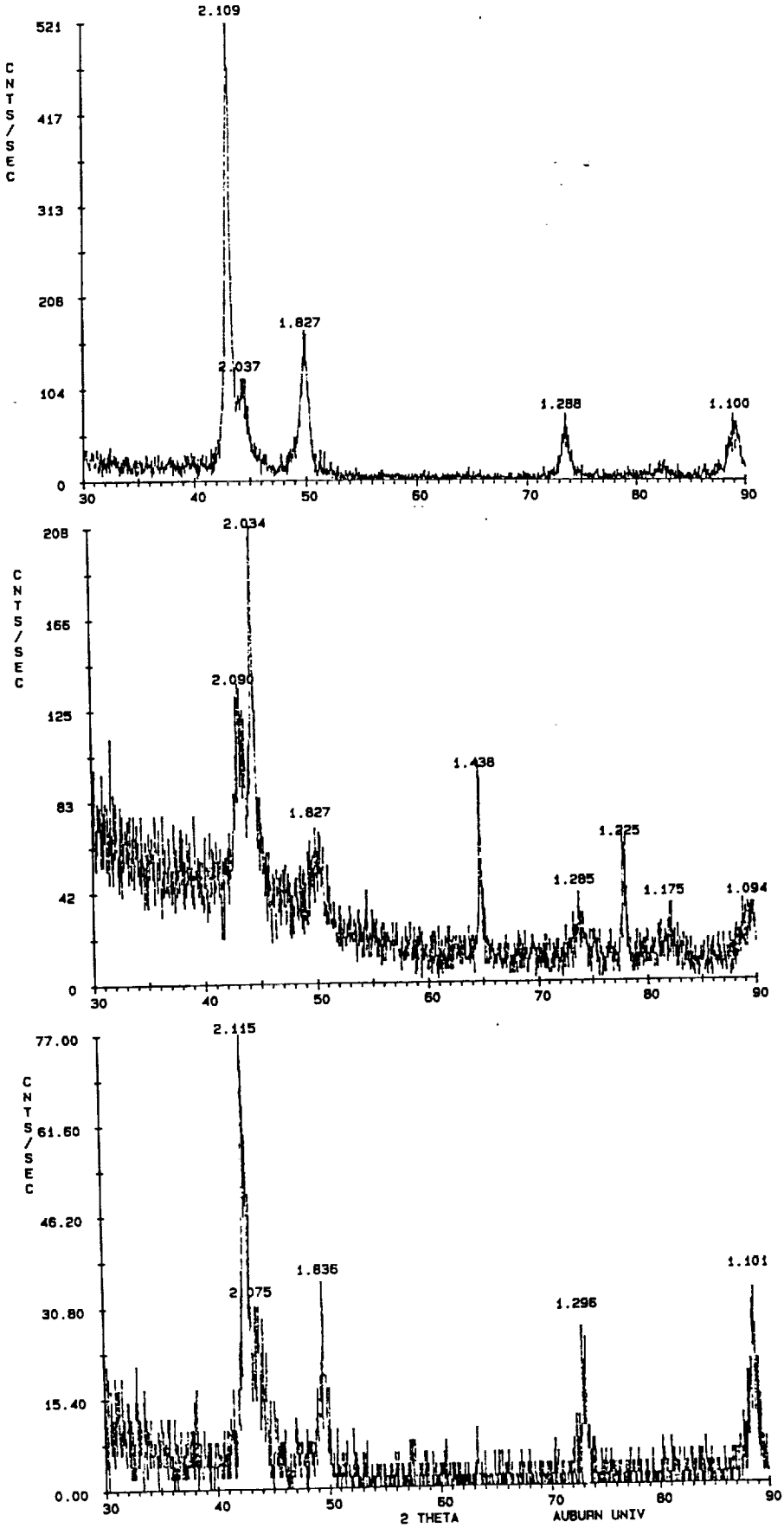

Figure 23. Diffraction patterns from specimen 16 taken from the longitudinal, long transverse and short transverse directions.

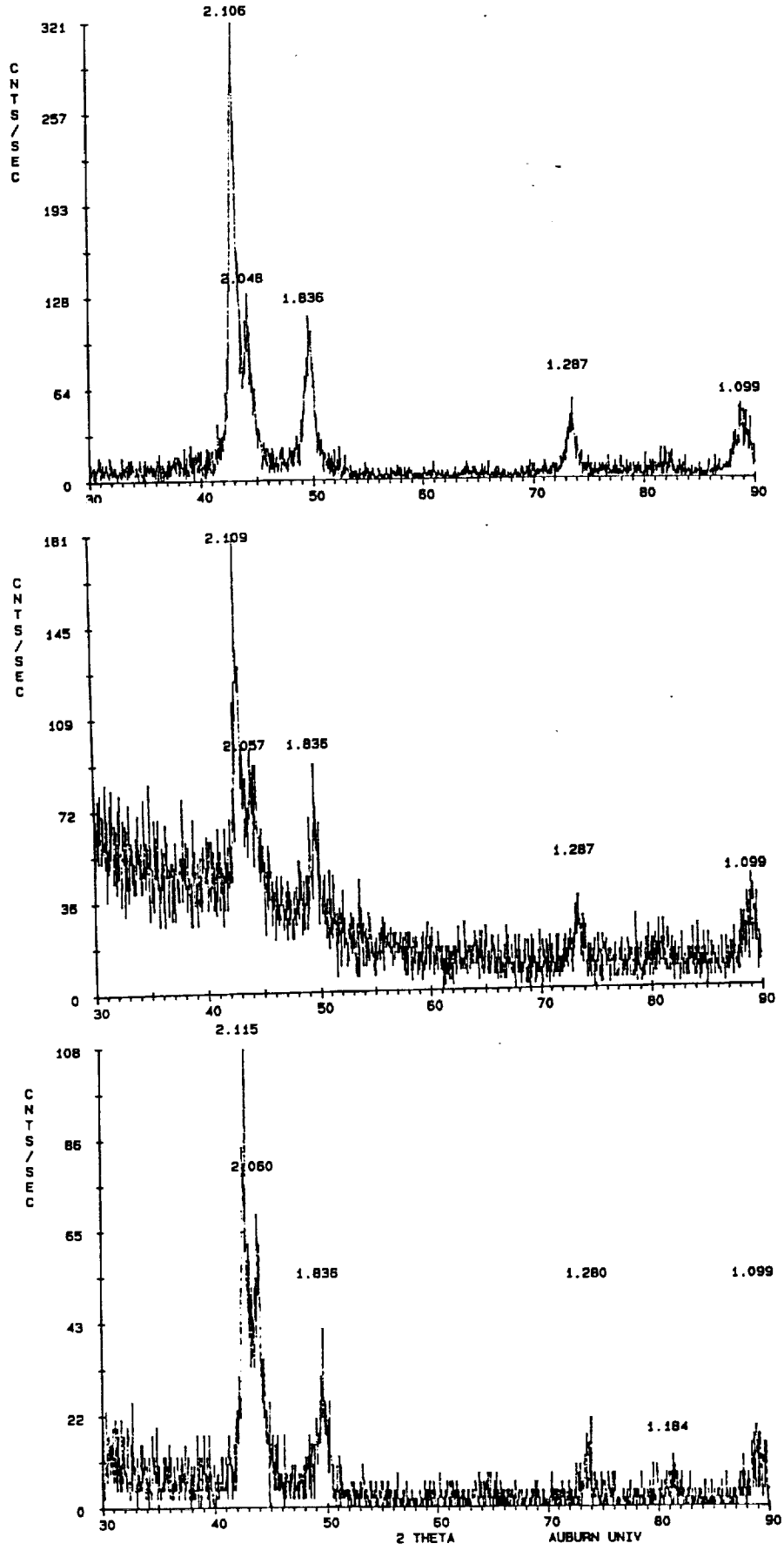

Figure 24. Diffraction patterns from specimen 17 taken from the longitudinal, long transverse and short transverse directions.

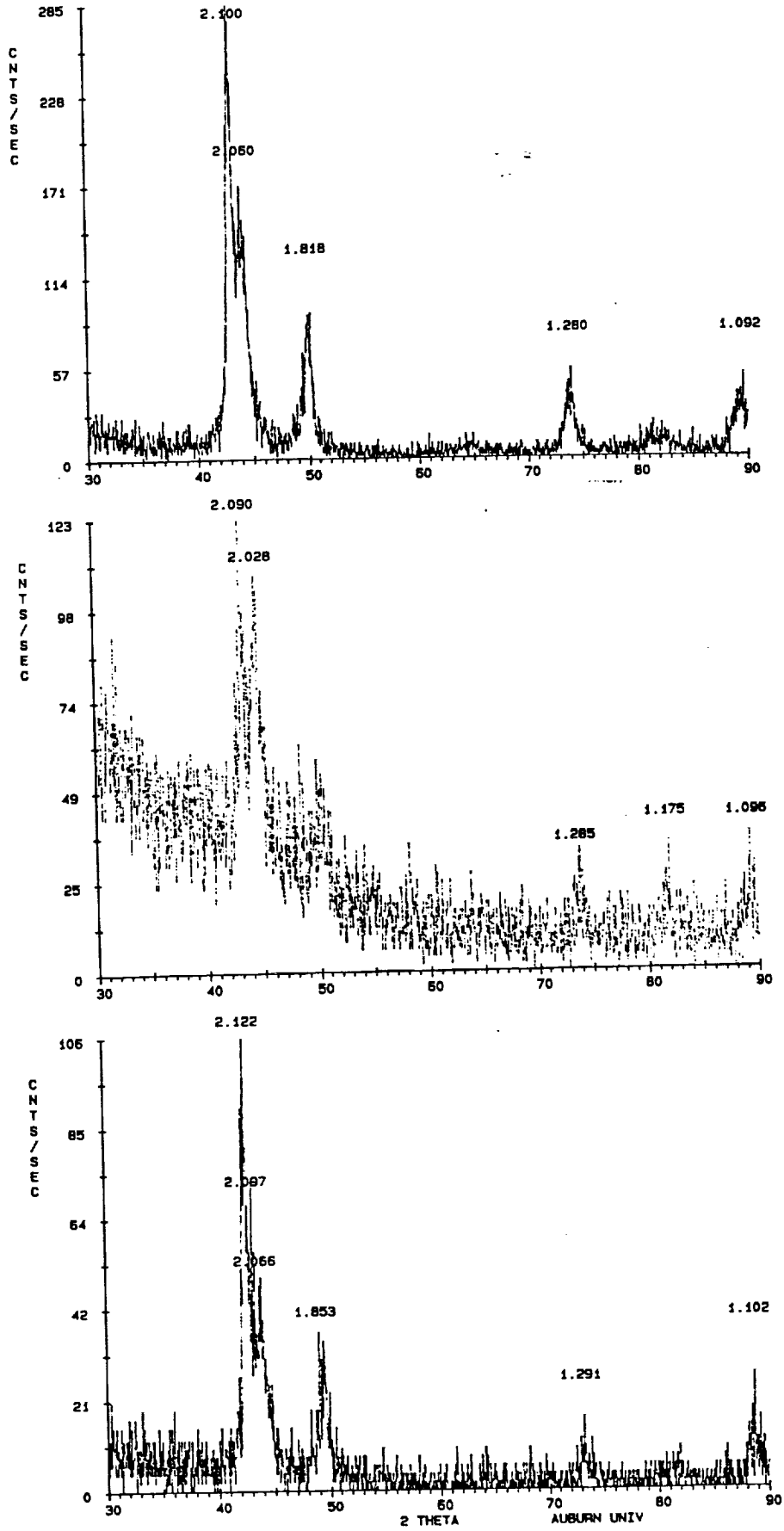

Figure 25. Diffraction patterns from specimen 18 taken from the longitudinal, long transverse and short transverse directions.

(a) Uniform cross section

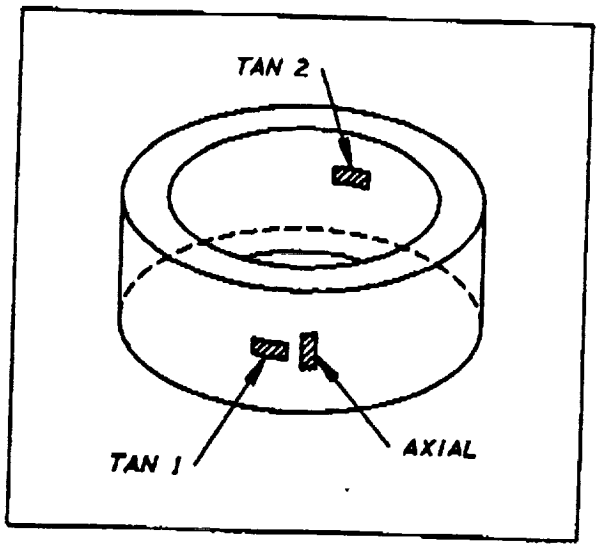

(b) Outer groove

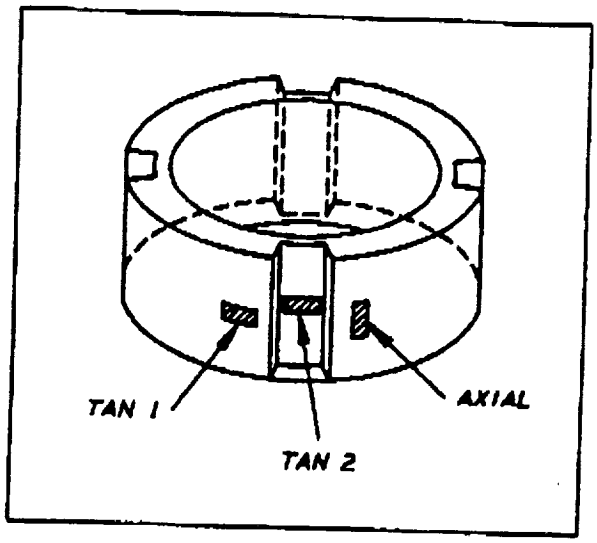

(c) Inner groove

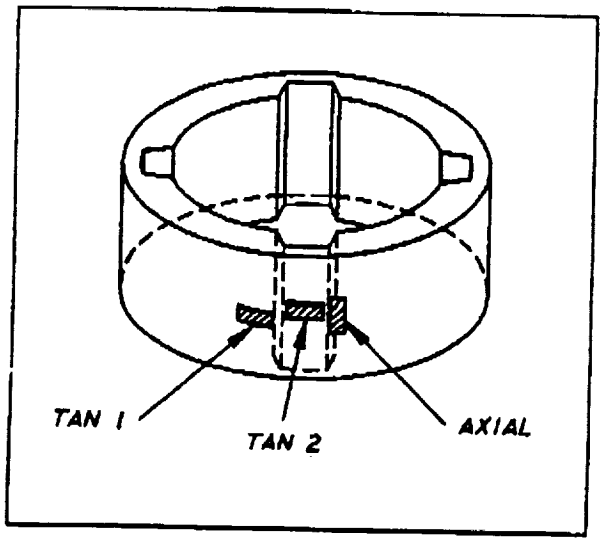

Figure 26. Ring geometries and the placement of strain gages.

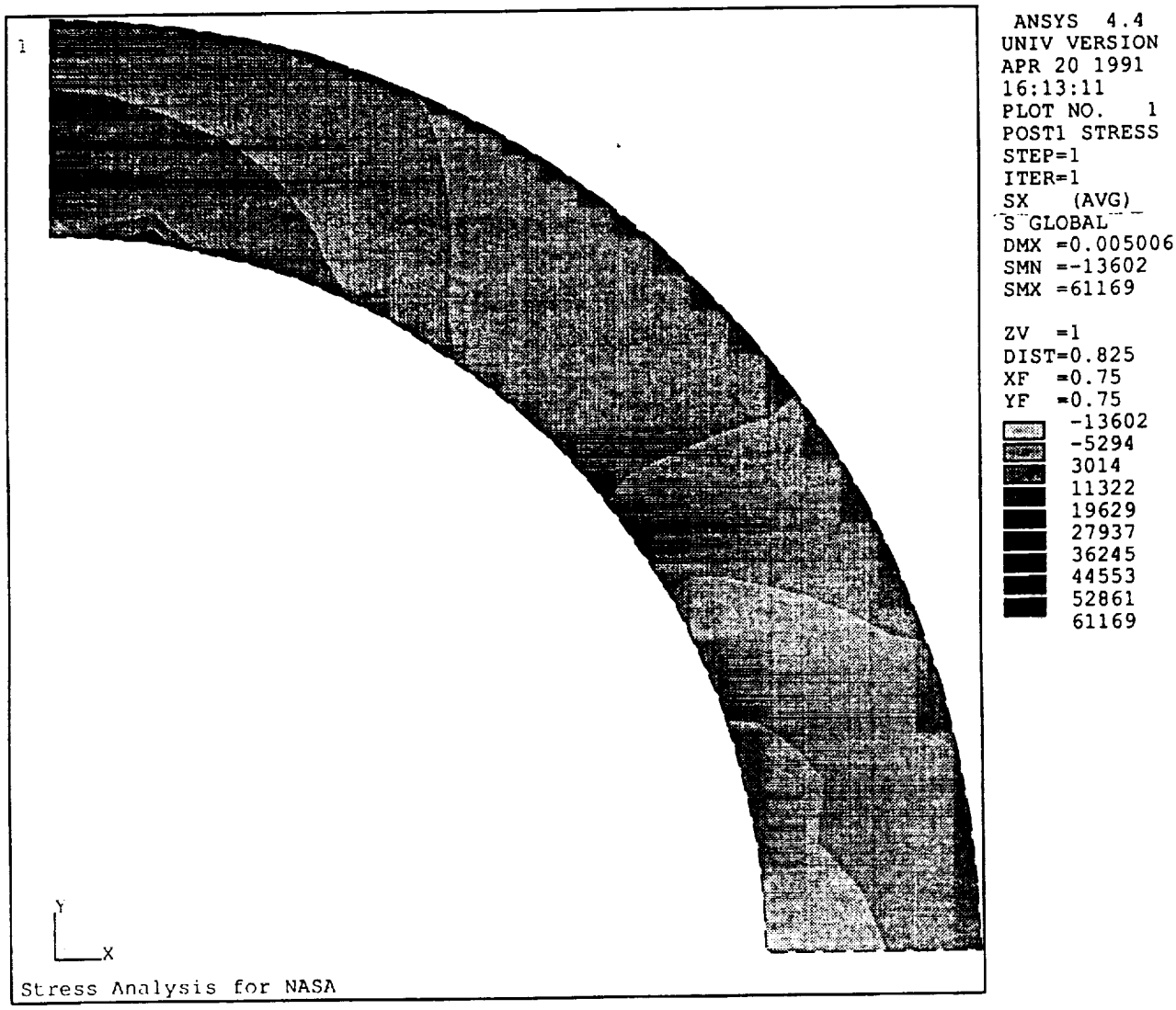

Figure 27. Stress in the x-direction in a uniform ring due to a radial displacement of 0.005" at the inner surface. The x-direction is horizontal. A maximum tangential stress of 60 ksi was induced at the top triangular region. The maximum radial stress obtained was only 14 ksi in compression.

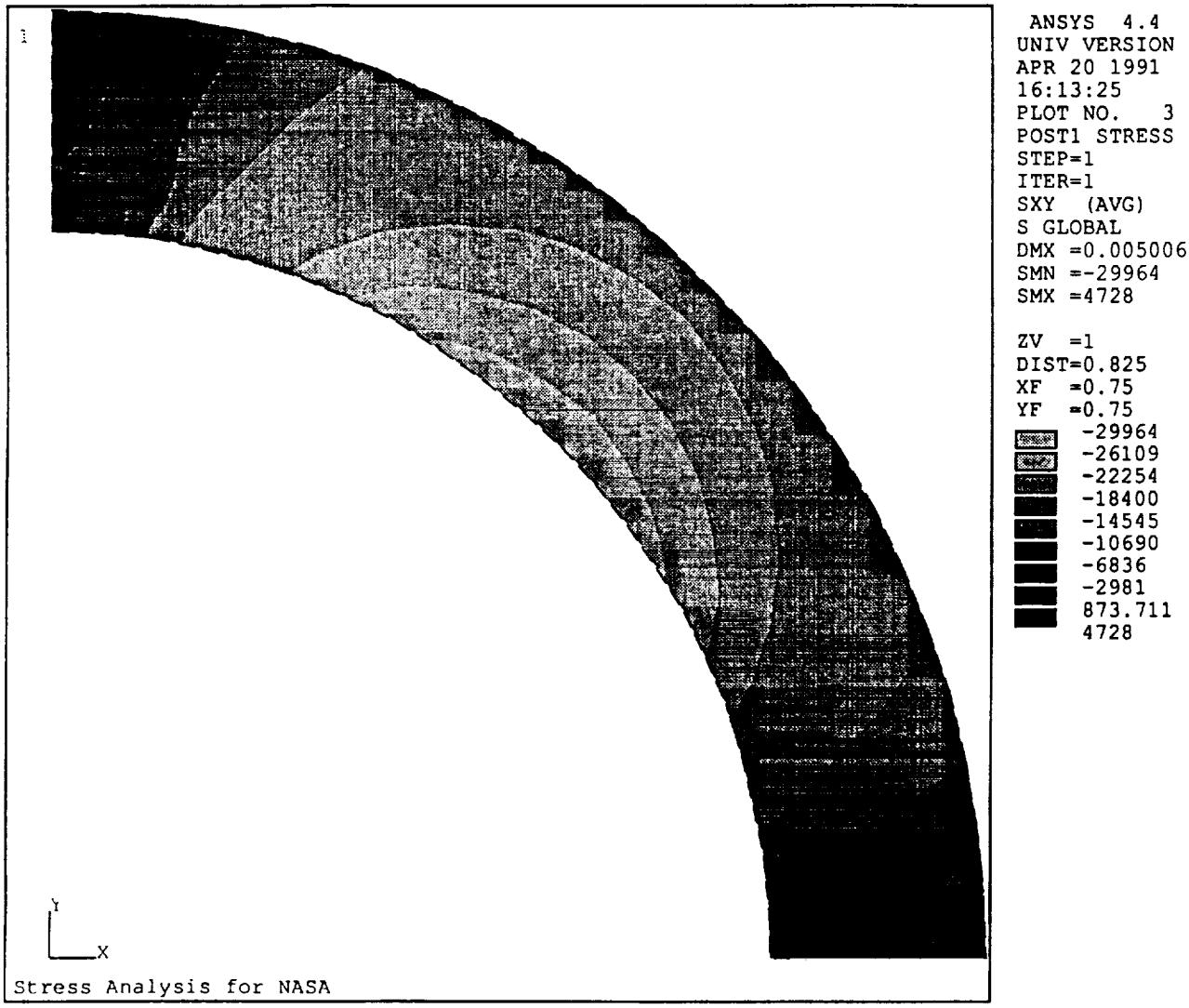

Figure 28. Distribution of shear stress in a uniform ring due to a radial displacement of 0.005" at the inner surface.

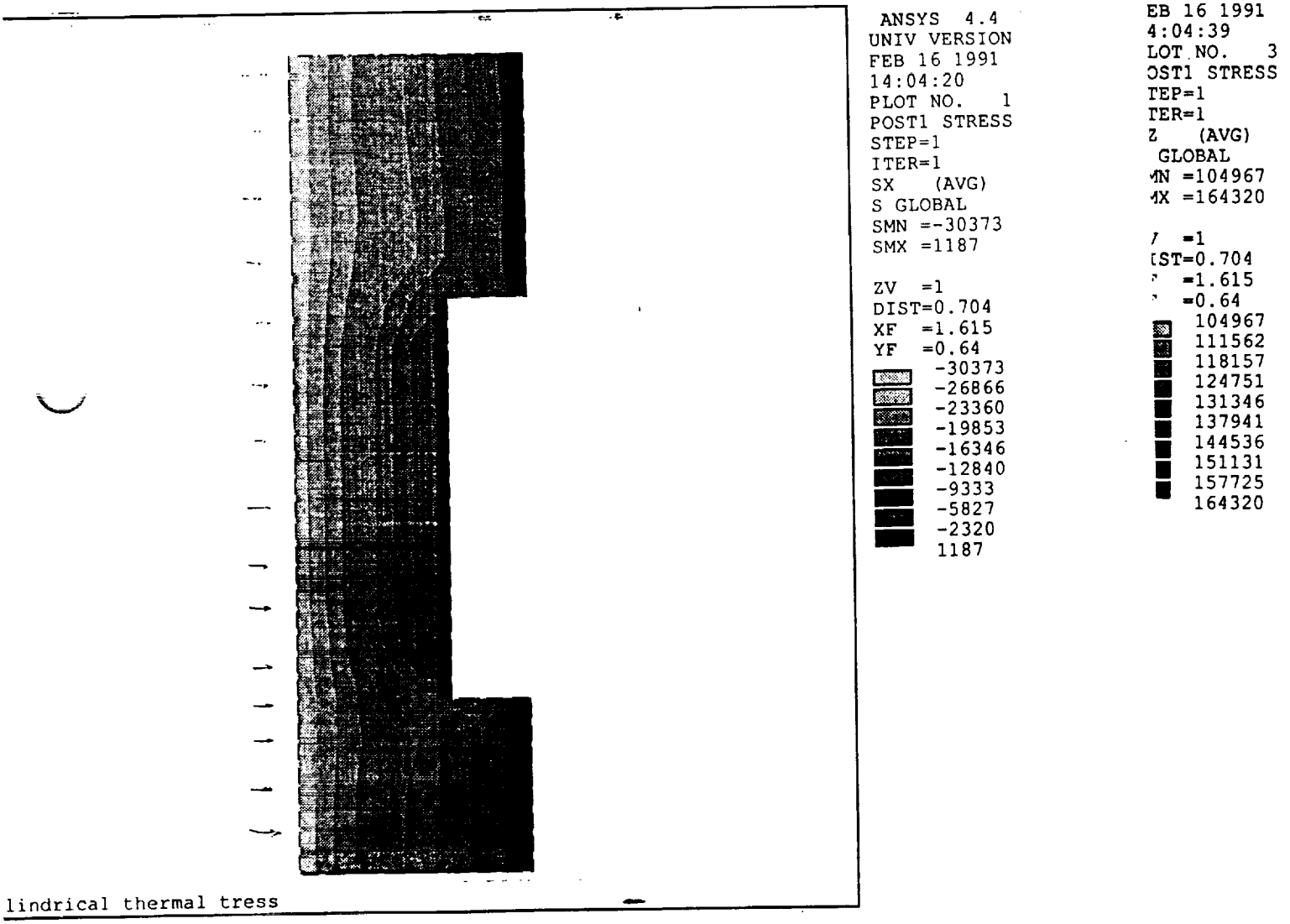

'igure 29. Distribution of radial stress in a ring with an inner race geometry due to an outward stress of 30 ksi applied to the inside of the ring.